

Overview of MiniBooNE

Ray Stefanski

Fermilab

August 29, 2010

An overview of backgrounds & systematic effects;
concentrating on ν interaction cross-section measurements

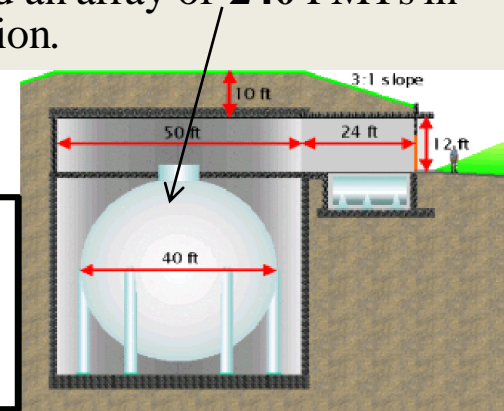
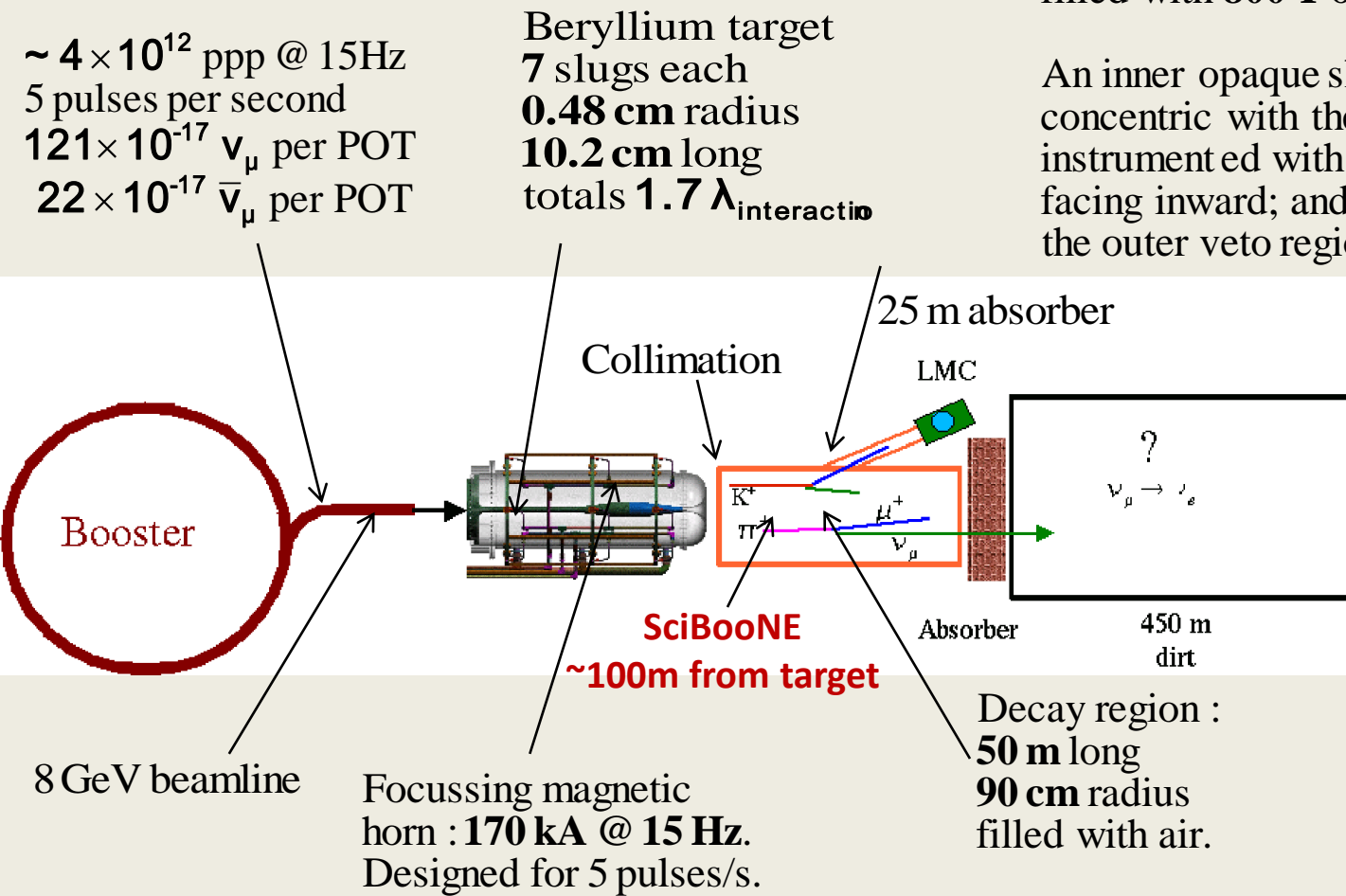
Rough Outline

- a.) detector configuration
- b.) sources of systematic uncertainty
 - b1.) flux
 - b2.) x-sections
 - b3.) reconstruction
- c.) MiniBooNE σ measurement
- d.) future

M'BooNE Schematic Geometry

The detector is a sphere of **610.6 cm** radius; located **541m** from target; filled with **800 T** of Marcol7 CH₂.

An inner opaque shell of radius **575 cm**, is concentric with the sphere and is instrumented with an array of **1280**, 8" PMTs facing inward; and an array of **240** PMTs in the outer veto region.



$$n = 1.47 \text{ -- } \beta_{\text{threshold}} = 0.68.$$

$$\rho = 0.86 \text{ g/cm}^3.$$

L/E ~1, similar to LSND

What constitutes an “event” in M’BooNE

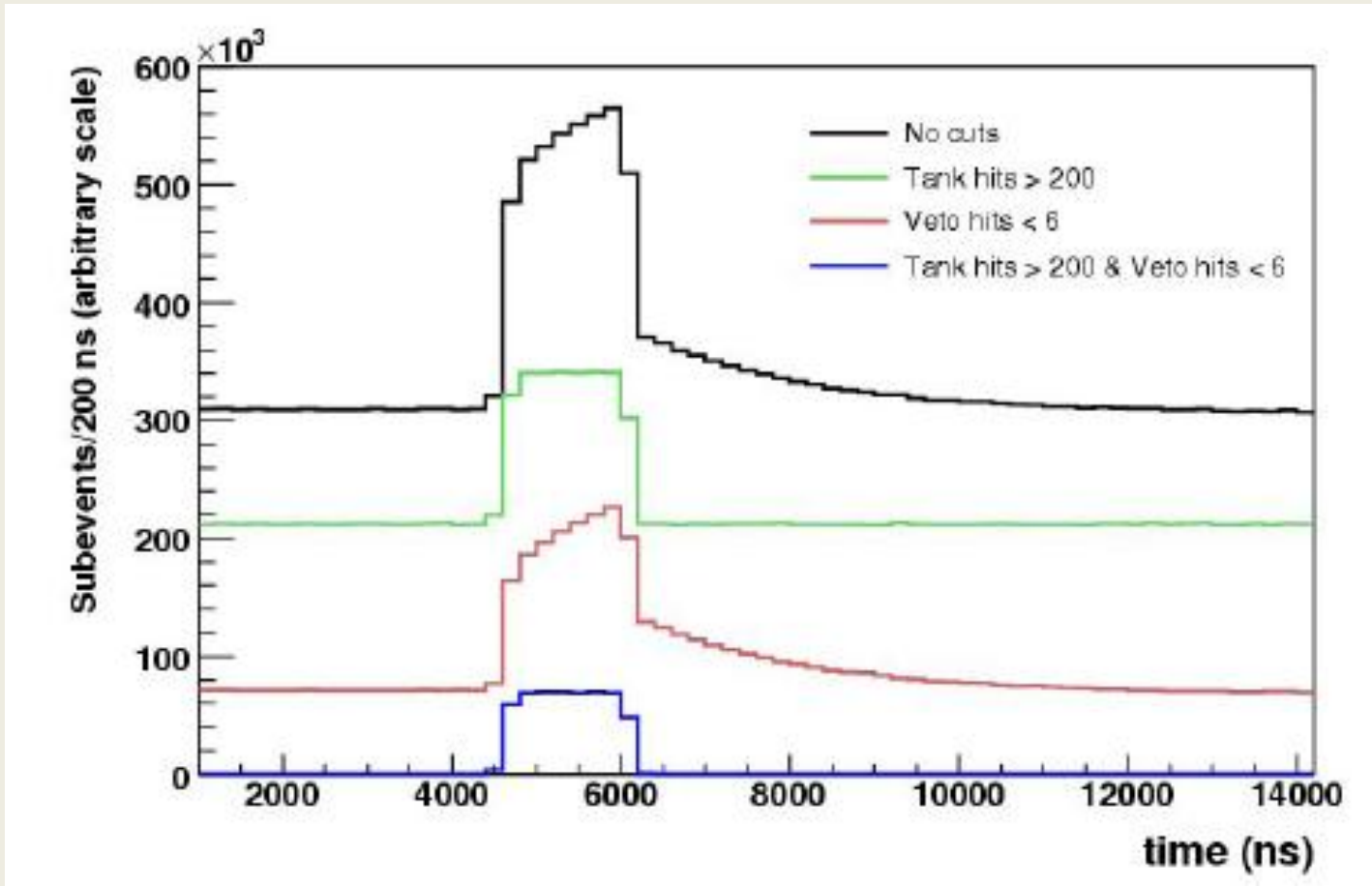
The ~ 1 GeV ν beam at M’BooNE results in interactions that are relatively low in outgoing multiplicity.

The largest interaction channel is the ν_l CCQE process $\nu_l + n \rightarrow \ell + p$, which accounts for $\sim 40\%$ of all the ν interactions in the M’BooNE detector.

Since the recoil proton is typically below β threshold, only the outgoing lepton, or π^0 for NC interactions, produces significant light.

While the recoiling nucleon can produce significant scintillation light, this additional source of light is not considered in the reconstruction.

What constitutes an “event” in M’BooNE

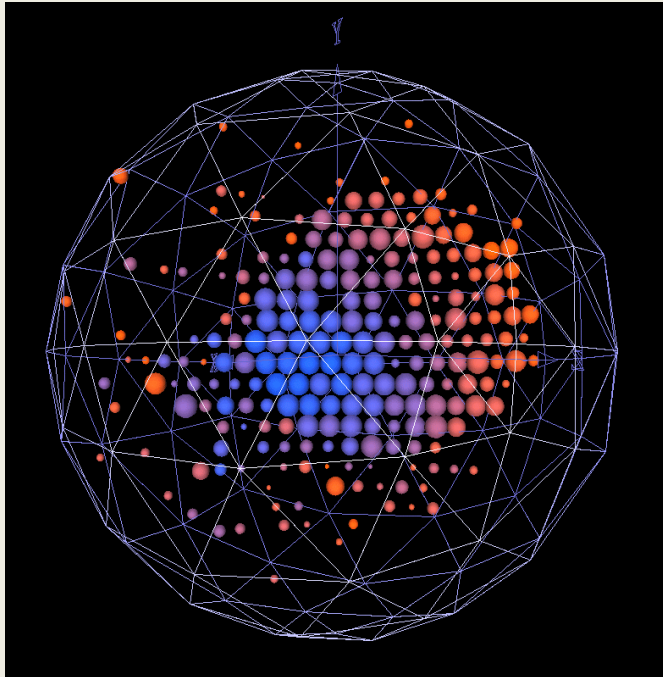


If we define a “hit” as a PMT with a signal above threshold, then we eliminate many backgrounds with a simple set of cuts.

What constitutes an “event” in M’BooNE

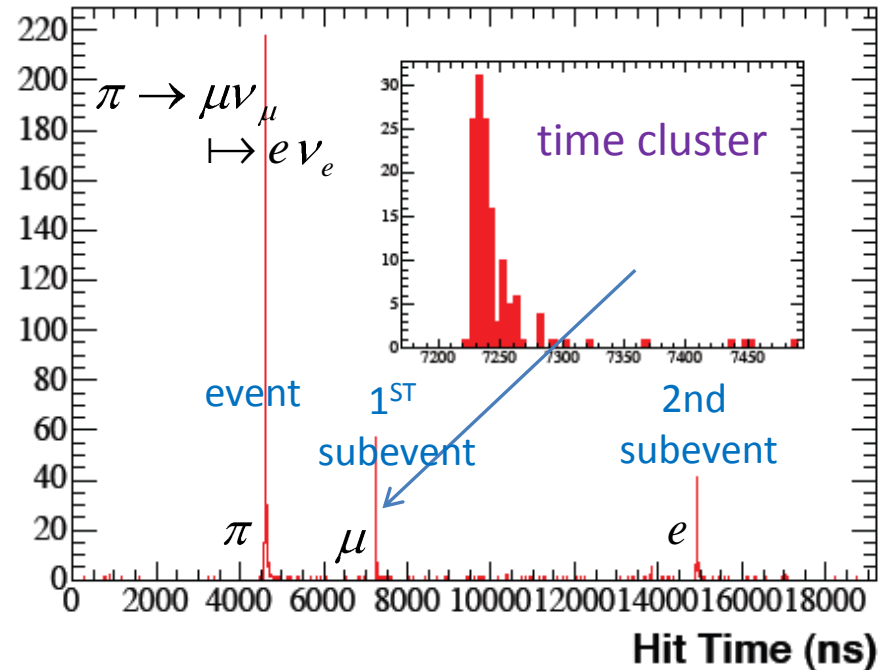
An event display:

- each bubble represents a PMT “hit”;
- charge -> bubble size;
- time -> color;
 - range is early;
blue comes later.



- PMT hits separated into time clusters
- Reconstruct Cherenkov rings and arrange in time.
 ν_μ CCQE events must contain 1 & only 1 subevent.

146,070 ν_μ CCQE events with 5.58×10^{20} POT
efficiency = 27%
purity = 77 %



Understanding the detector: response of the oil to γ

γ Creation

A1. Cherenkov light

β dependence

A2. Scintillation

a. dE/dx

b. temporal response

Run time measurements

- Michel electrons A1; A2; B2
- Cosmic muons A1; A2; B2
- Diffuse laser light B1; B2
- Pencil beam laser B1; B2

γ Propagation

B1. Scattering (Rayleigh)

a. temporal response (prompt)

b. $1 + \cos^2 \theta$

c. λ^4 dependence

B2. Fluorescence

a. isotropy

b. temporal response

c. λ dependence

B3. Absorption

Measurement of the properties of the oil.

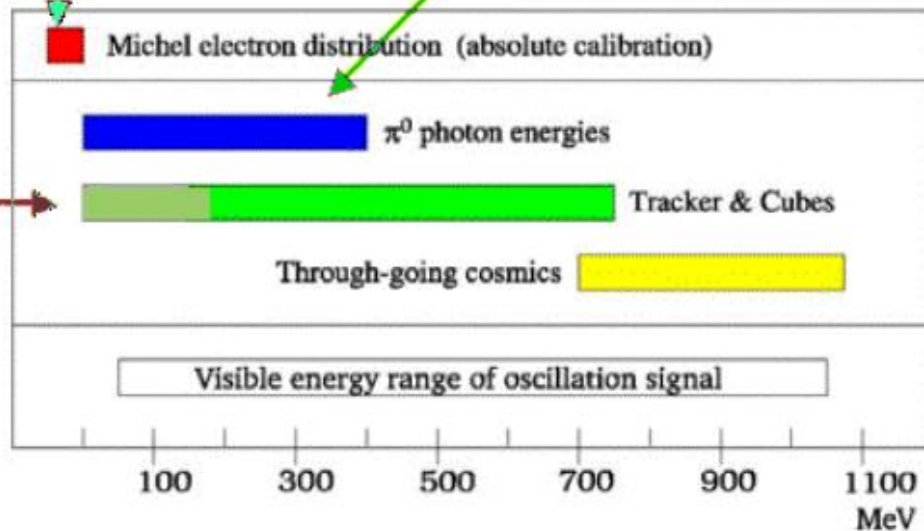
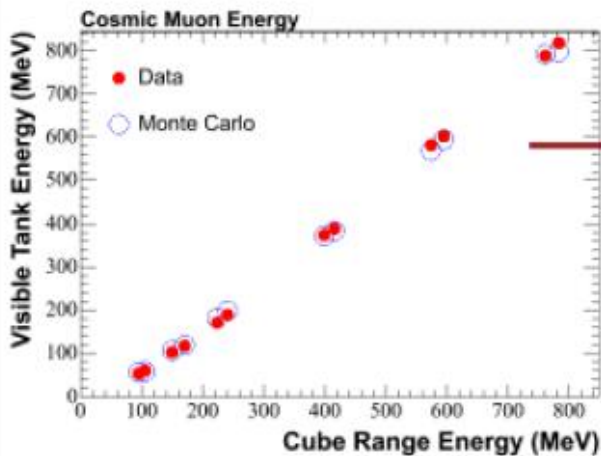
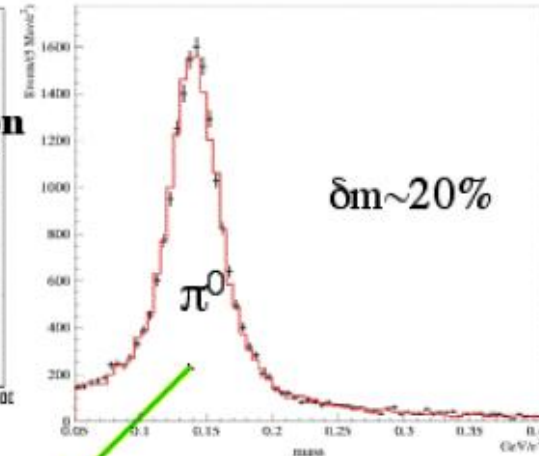
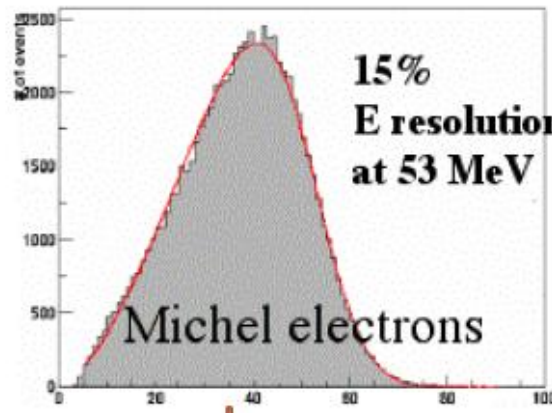
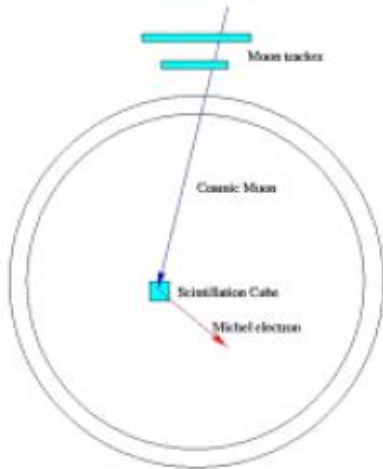
- Scintillation (IUCF) w/p⁺ A2
- Scintillation (Fermilab) w/ μ A2
- repeated w/p⁺ (IUCF)
- Goniometry (Princeton) B1; B4
- Fluorescence spectroscopy (Fermilab) B2
- Temporal spectroscopy (JHU) B2
- Attenuation (Fermilab) B1; B2; B3
- multiple devices

Understanding the detector: Energy dependence

Calibration Sources

Cube	$\langle T_\mu \rangle$	$\delta \langle T_\mu \rangle$
Depth		
(cm)	(MeV)	(MeV)
31.3	95	4
60.3	155	5
100.5	229	7
200.8	407	9
298.1	584	9
401.9	771	9

Tracker system

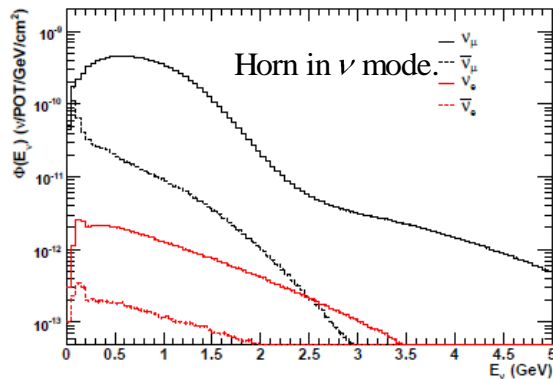


Understanding the detector: Flux uncertainties – particle production

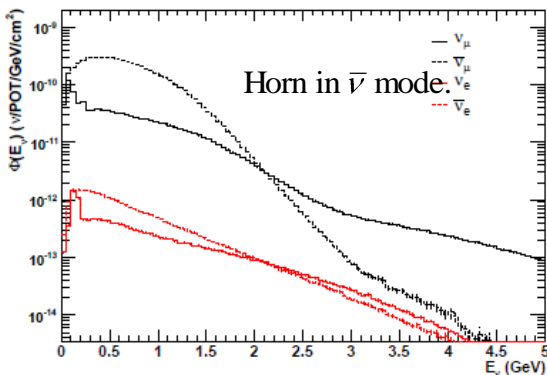
Geant4 - based neutrino flux simulation.

From ν_μ CCQE interactions, measured flux exceeds prediction by 1.21 ± 0.24

Simulation includes tertiary interactions in target area and decay volume.



From $\bar{\nu}_\mu$ CCQE interactions, measured flux roughly equals predicted flux.



These are the M' BooNE published production π uncertainties based on a 9 parameter fit of the Sanford - Wang formula to the HARP measurements, extended to account for thick target effects.

In practice, flux error uncertainties are derived from a spline fit to the HARP data, which result in a $\sim 9\%$ error at the peak flux at ~ 800 MeV energy. The complete error matrix is calculated in bins of ν energy and include correlations between bins.

Horn in ν mode.

Source of Uncertainty	ν_μ	$\bar{\nu}_\mu$	ν_e	$\bar{\nu}_e$
Proton delivery	2.0%	2.0%	2.0%	2.0%
Proton optics	1.0%	1.0%	1.0%	1.0%
π^+ production	14.7%	1.0%	9.3%	0.9%
π^- production	0.0%	16.5%	0.0%	3.5%
K^+ production	0.9%	0.2%	11.5%	0.3%
K^0 production	0.0%	0.2%	2.1%	17.6%
Horn field	2.2%	3.3%	0.6%	0.8%
Nucleon cross sections	2.8%	5.7%	3.3%	5.6%
Pion cross sections	1.2%	1.2%	0.8%	0.7%

Horn in $\bar{\nu}$ mode.

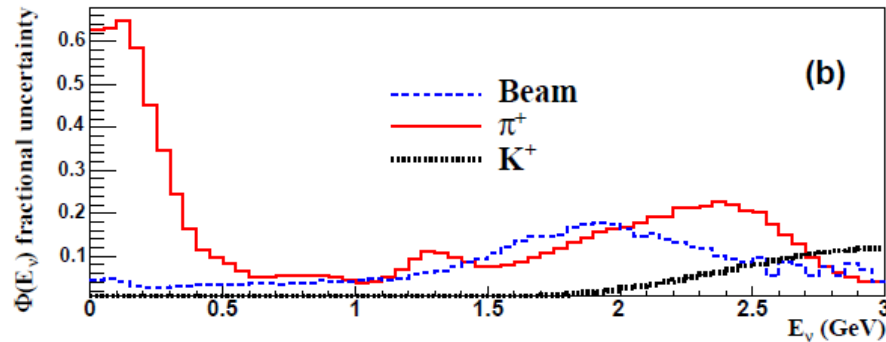
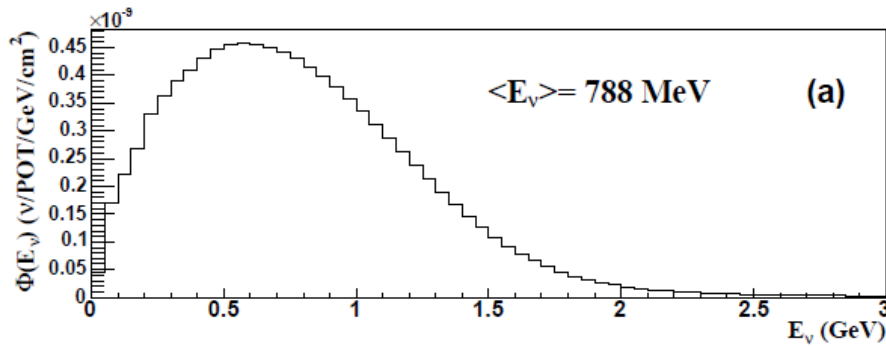
Source of Uncertainty	ν_μ	$\bar{\nu}_\mu$	ν_e	$\bar{\nu}_e$
Proton delivery	2.0%	2.0%	2.0%	2.0%
Proton optics	1.0%	1.0%	1.0%	1.0%
π^+ production	13.8%	0.1%	2.1%	0.1%
π^- production	0.5%	17.5%	0.0%	13.6%
K^+ production	3.1%	0.0%	22.3%	0.4%
K^0 production	0.1%	0.0%	6.1%	3.9%
Horn field	1.5%	1.0%	3.2%	1.5%
Nucleon cross sections	6.2%	2.1%	6.2%	2.5%
Pion cross sections	1.5%	1.2%	1.6%	1.5%

Understanding the detector: Flux uncertainties – beam properties

Change in flux from π^+ due to dominant sources of systematic uncertainty:
 horn current;
 n-N qe x-sect.;
 π^+ -N qe x-sect..

increased

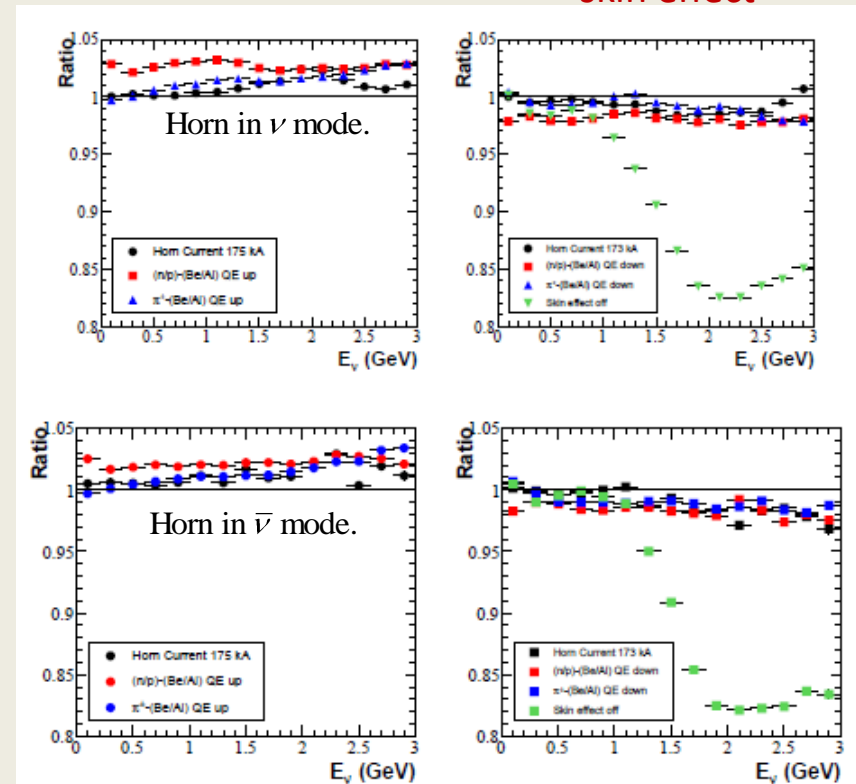
decreased &
skin effect



(a) Predicted ν_μ flux at the M' BooNE detector.

(b) Fractional uncertainties grouped into various contributions.

The integrated flux is $5.15 \times 10^{-10} \nu_\mu/\text{POT}/\text{cm}^2$ ($0 < E_\nu < 3 \text{ GeV}$) with mean energy of 788 MeV.



Understanding the detector: cross-sections – NUANCE

Predictions from the NUANCE event generator for fractional occurrence of ν_μ interactions in neutrino mode. Resonant and coherent processes are included.

neutrino process	abbreviation	reaction	fraction (%)
CC quasielastic	CCQE	$\nu_\mu + n \rightarrow \mu^- + p$	39
NC elastic	NCE	$\nu_\mu + p(n) \rightarrow \nu_\mu + p(n)$	16
CC $1\pi^+$ production	CC $1\pi^+$	$\nu_\mu + p(n) \rightarrow \mu^- + \pi^+ + p(n)$	25
CC $1\pi^0$ production	CC $1\pi^0$	$\nu_\mu + n \rightarrow \mu^- + \pi^0 + p$	4
NC $1\pi^\pm$ production	NC $1\pi^\pm$	$\nu_\mu + p(n) \rightarrow \nu_\mu + \pi^\pm (\pi^-) + n(p)$	4
NC $1\pi^0$ production	NC $1\pi^0$	$\nu_\mu + p(n) \rightarrow \nu_\mu + \pi^0 + p(n)$	8
multi pion production, DIS, etc.	other	$\nu_\mu + p(n) \rightarrow \mu^- + N\pi^\pm + X, \text{ etc.}$	4

Constants used in NUANCE models :

M_A^{QE}	$= 1.35 \pm 0.17;$	axial mass for QE and NCEL events
E_B	$= 34 \text{ MeV} \pm 9 \text{ MeV};$	binding energy in Fermi gas model
p_F	$= 220 \text{ MeV}/c \pm 30 \text{ MeV};$	Fermi momentum in Fermi gas model
Δ_s	$= 0 \pm 0.10;$	strange contribution to proton spin
$MA_{1\pi}$	$= 1.1 \text{ GeV} \pm 0.275 \text{ GeV};$	axial mass in resonant 1π production mode
$MA_{N\pi}$	$= 1.3 \text{ GeV} \pm 0.52 \text{ GeV};$	axial mass in $N\pi$ and non - pion production mode
cog	$= 1; \text{ NC}$	coherent π^0 cross - section
delrad	$= 1.022 \pm .1245;$	Δ radiative ($\Delta \rightarrow N\gamma$) BF and π FSI.
dis	$= 1 \pm 0.25;$	DIS cross - section - - not well known at MiniBooNE energies.
kappa	$= 1.007 \pm 0.012;$	Pauli blocking scale factor
macoh	$= 1.03 \text{ GeV} \pm 0.275;$	axial mass in NC, CC coherent pion production x - sections.
RES pi0	$= 0.947;$	NC resonant π^0 cross - section
$MA_{\text{QE}}^{\text{H}}$	$= 1.13 \pm 0.10;$	axial mass for QE and NC EL interactions on H_2
Nubar	$= 1.0 \pm 0.10;$	cross - section normalization uncertainty for $\bar{\nu}$ scattering

Variables extracted from the track reconstruction assuming a μ hypothesis.

T_μ = muon kinetic energy

θ_μ = muon scattering angle.

Additional reported observables are :

$E_\mu = T_\mu + m_\mu$ the total muon energy

$$E_\nu^{\text{QE}} = \frac{2(M_n')E_\mu - ((M_n')^2 + m_\mu^2 - M_p^2)}{2 \cdot [(M_n') - E_\mu + \sqrt{E_\mu^2 - m_\mu^2} \cos \theta_\mu]},$$

$$Q_{\text{QE}}^2 = -m_\mu^2 - 2E_\nu^{\text{QE}}(E_\mu - \sqrt{E_\mu^2 - m_\mu^2} \cos \theta_\mu),$$

where $M_n, M_p,$ and m_μ are the neutron, proton and muon masses.

$M_n' = M_n - E_B,$ where E_B is the separation energy in carbon and is set to $34 \pm 9 \text{ MeV}.$

A similar set of relations is used for electrons and photons.

Understanding the detector: event reconstruction

In the track based reconstruction, four signal patterns are used:

1. single electron track,
2. single muon track,
3. two γ tracks,
4. and two γ tracks with a π^0 invariant mass.

The CH_2 has an extinction length of $\sim 20\text{m}$, the radiation length is $\sim 50\text{cm}$, and exhibits a wide range of optical phenomena near the peak of the PMT sensitivity: 400 nm.

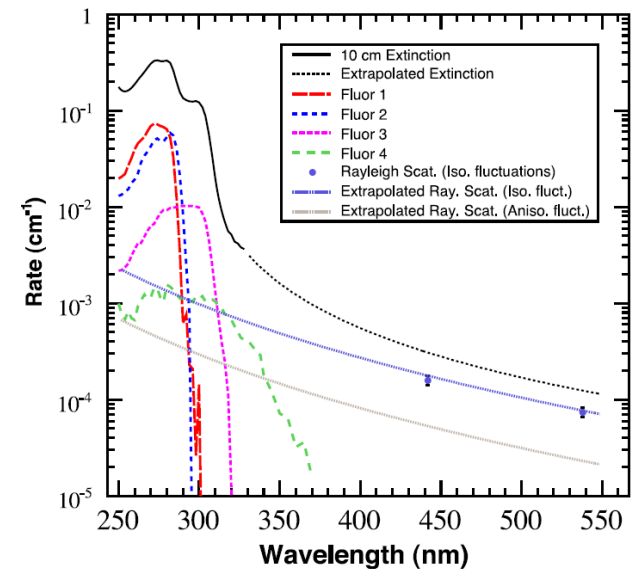
Cherenkov light and scintillation light are accompanied by

1. photon absorption;
2. fluorescence; (with several excitation/emission spectra and lifetimes)
3. Rayleigh scattering;
4. and Raman scattering.

Also, photon reflection from the surface of the tubes, and the surface of the main detector region must be considered in the simulations.

The electronics dead time is ~ 300 ns.

A Geant3-based Monte Carlo simulation serves as the main tool for developing reconstruction algorithm's predictive models.



Understanding the detector: event reconstruction

The quantities measured by the detector are:
the number of PMTs that have recorded a light pulse – “hits” –
the charge recorded on each PMT; and the time of the hit.

From these measured quantities,
a vector with seven variables, \mathbf{x} ,
is produced :

- The starting point : x_0, y_0, z_0 ;
- The starting time : t_0 ;
- the direction : θ_0, ϕ_0 ;
- The kinetic energy : E_0 .

In simulation, the flux, cross-section model (NUANCE), and detector characteristics are combined to convert an event type as input to generation of a set of PMT hits with associated time and charge. The simulation and data are passed through the same reconstruction routines to generate \mathbf{x} , which is used to test our ability to reproduce the data in simulation.

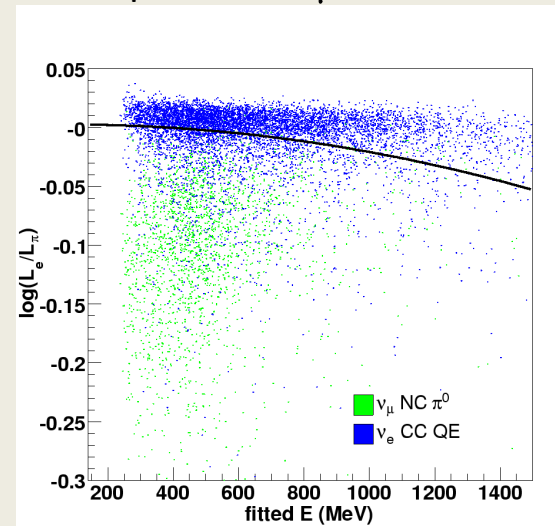
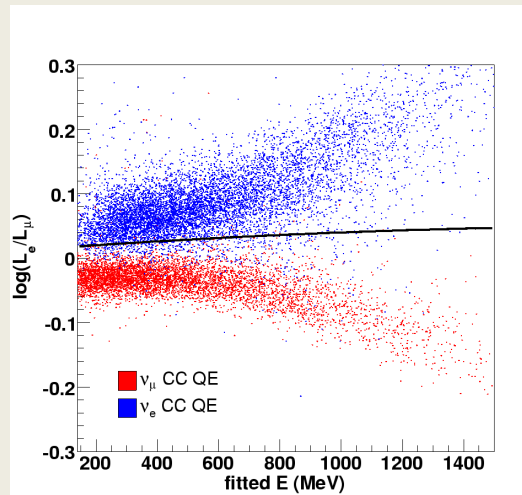
MiniBooNE event reconstruction – particle identification:

The process leads to the development of negative log-likelihoods for each of the fitted hypothesis. If \mathcal{L}_e , \mathcal{L}_μ , and \mathcal{L}_π are the maximized likelihoods returned by the electron, muon, and (fixed-mass) two-track fits, respectively, then the ratios

$$\mathcal{R}_{e/\mu} = \log \mathcal{L}_e - \log \mathcal{L}_\mu \text{ and}$$

$$\mathcal{R}_{e/\pi} = \log \mathcal{L}_e - \log \mathcal{L}_\pi,$$

can be used as a test of the electron hypothesis, compared to a μ or π^0 .



The events undergo pre-selection based on:

- only one time cluster is present in the event, to eliminate Michel electrons from μ decay.
- more than 200 hits in the main detector, to eliminate cosmic rays,
- less than 6 hits in the veto region also to eliminate cosmic rays.
- the event must also occur in the Booster beam window.

cross sections: Llewellyn Smith

$$\frac{d\sigma}{dQ^2} = \frac{G_F^2 M}{8\pi E_\nu^2} \left[A \mp \frac{s-u}{M^2} + \frac{(s-u)^2}{M^4} C \right],$$

where, (+) - refers to (anti)neutrino scattering, Q^2 is the squared 4 - momentum transfer, G_F is the Fermi constant, M is the nucleon mass, E_ν is the incident neutrino energy, and $(s-u) = 4ME_\nu - Q^2 - m_l^2$ with m_l the mass of the charged lepton produced in the interaction. The Q^2 dependence is explicit in the parameters A , B , C .

$$A = \frac{(m_l^2 + Q^2)}{M^2} [(1+\tau)F_A^2 - (1-\tau)F_1^2 + \tau(1-\tau)F_2^2 + 4\tau F_1 F_2 - m_l^2 - \frac{m_l^2}{4M^2} [(F_1 + F_2)^2 + (F_A + 2F_P)^2 - 4(1+\tau)F_P^2]]$$

$$B = \frac{Q^2}{M^2} F_A (F_1 + F_2)$$

$$C = \frac{1}{4} (F_A^2 + F_1^2 + F_2^2),$$

where $\tau = \frac{Q^2}{4M}$. The two vector form factors, F_1 and F_2 , are given by

$$F_1 = \frac{1 + \tau(1 + \mu_p - \mu_n)}{(1 + \tau)(1 + Q^2/m_l^2)^2}, \text{ and } F_2 = \frac{(\mu_p - \mu_n)}{(1 + \tau)(1 + Q^2/m_l^2)^2},$$

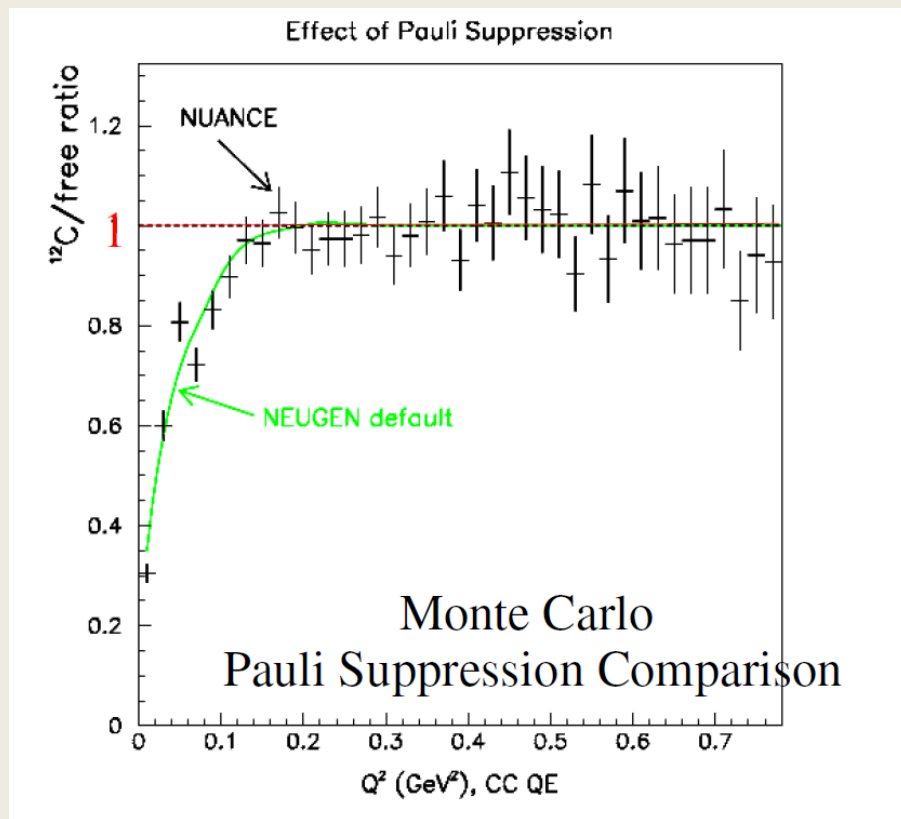
$$F_A = g_A / \left(1 + \frac{Q^2}{M_A^2}\right), \text{ and } F_P = \frac{2M^2}{m_\pi^2 + Q^2},$$

where m_π is the pion mass, μ_p and μ_n are the proton and neutron anomalous magnetic moments, and M_V , g_A , and M_A are empirical parameters.

The Q^2 dependence of the vector form factors, F_1 and F_2 are measured in precision electron scattering experiments. Neutron beta decay fixes the value of $g_A = -1.267$.

M_A is determined from neutrino scattering experiments.

cross-sections: Pauli suppression

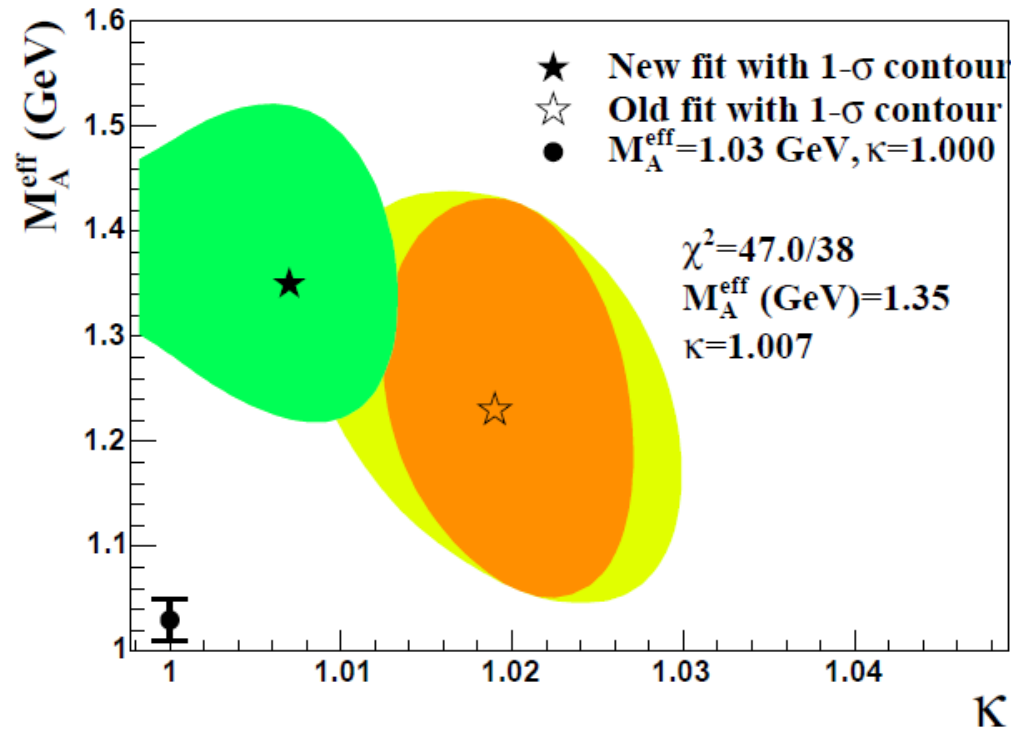


In the RFG model, “Pauli-blocking” causes a suppression in the cross-section for low values of the momentum transfer, Q^2 .

The struck nucleon is forbidden from entering a state already occupied by one of the spectator nucleons in the interaction. In the previous slide, the CCQE σ prediction on neutrons bound in carbon using this model. κ is a measure of the Pauli-blocking, and is normally set to 1.

To get out of the nucleus, the final state lepton must have $p > p_F$

M_A^{eff} and κ



Shape - only fit to 2
subevent sample
yields model parameters :
 $M_A^{\text{eff}} = 1.35 \pm 0.17$ GeV/c²
 $\kappa = 1.007 \pm 0.012$;
 $\chi^2 / dof = 47.0 / 38$.

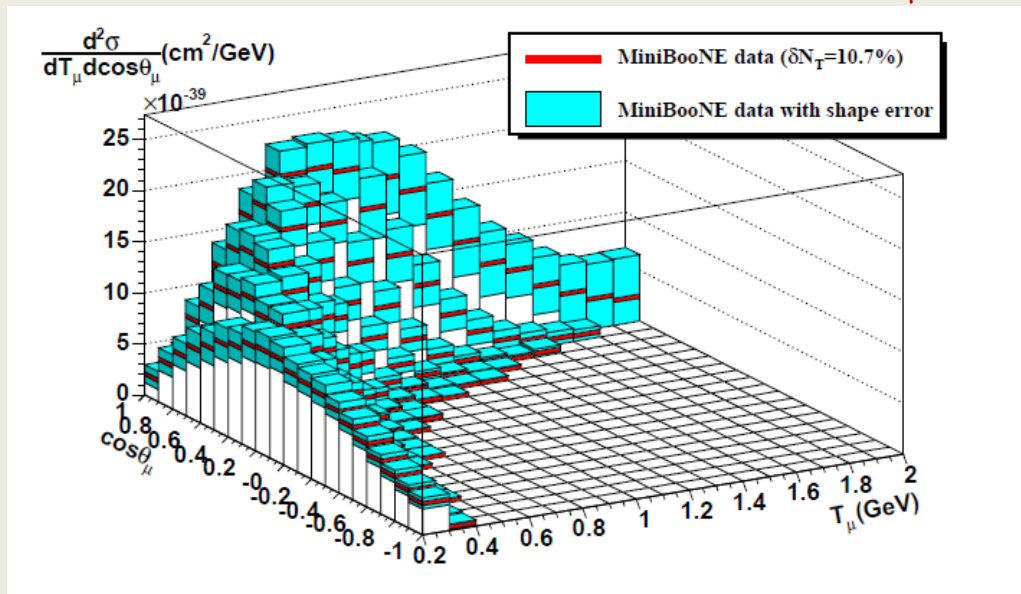
2 error ellipses are shown
for the previous work – the
larger is the total uncertainty
included in the previous
paper.

A 1 σ contour plot for M_A^{eff} vs. κ . The filled star is the best fit point and contour extracted from this work. The open star indicates the best fit point and contour from the previous work. The circle indicates the best world-average value for M_A .

Results: cross sections:

Provide differential cross-sections, correctly normalized with a predicted ν flux (not normalized to a different reaction channel in the same data).

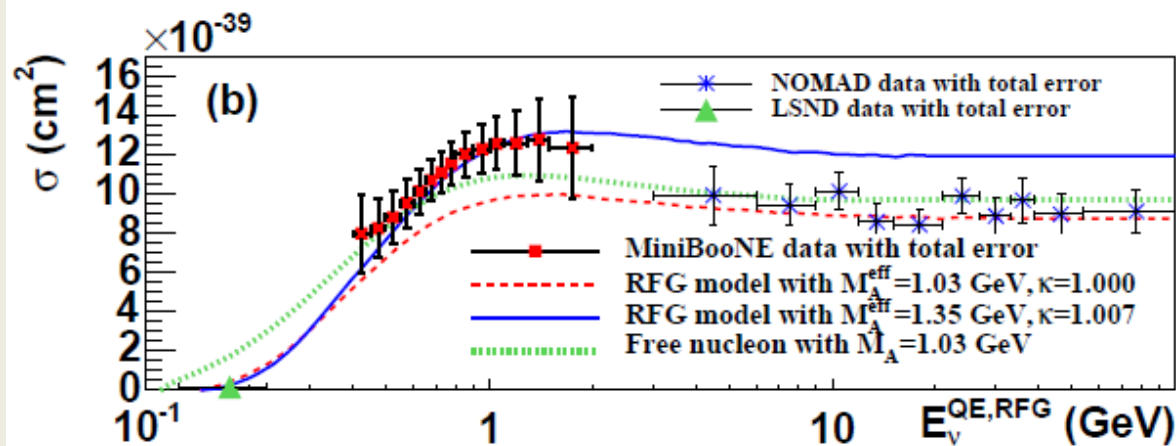
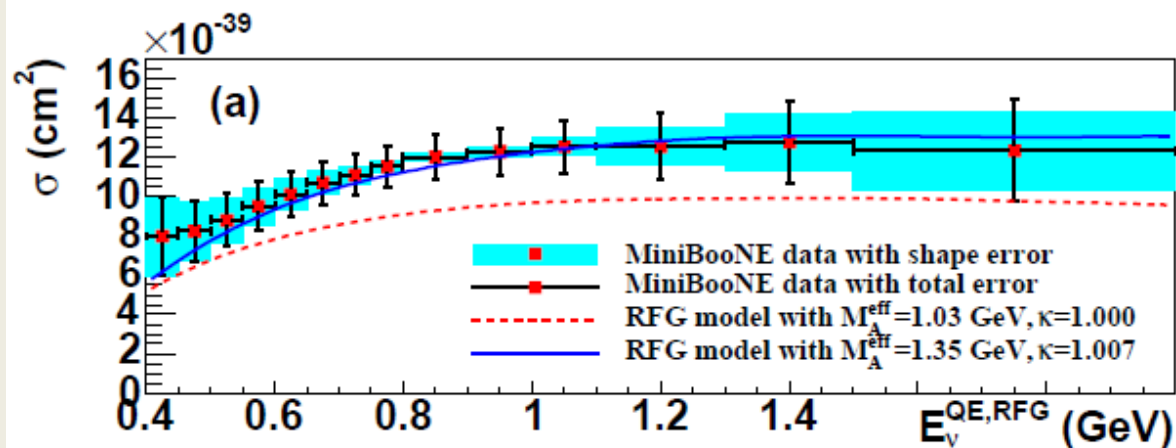
Based on the world's largest sample of ν_μ CCQE events (~150,000) @ 1 GeV region.



Flux integrated double differential cross section per target neutron for the ν_μ CCQE process. Dark bars represent measured values, and the lighter bands represent the shape errors.

source	normalization
	error
	(%)
ν flux prediction	8.66
background x-sections	4.32
detector model	4.6
kinematic unfolding process	0.6
statistics	0.26
total	10.7

Results: cross sections



Flux – unfolded ν_{μ} CCQE σ per neutron as a function of ν Energy.

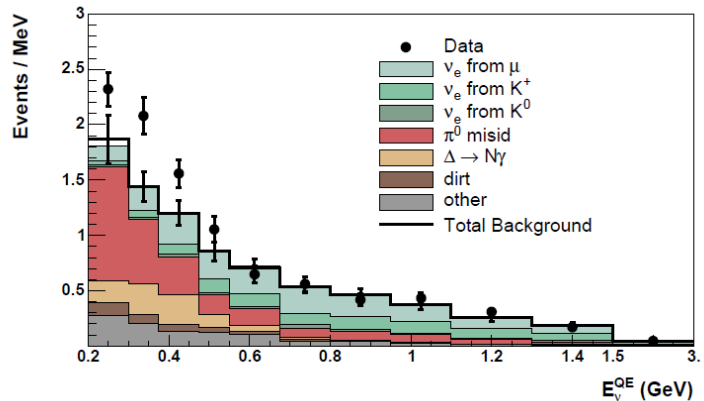
In (a), shape errors are shown as shaded boxes along with the total error bars.

In (b), a larger energy range is shown along with results from LSND, and NOMAD.

Also shown are predictions for a RFG model with 2 different parameter variations and for scattering from free nucleons.

ν appearance

2 independent blind analyses were performed:
 Track Based Analysis (TBA); Boosted Decision Tree (BDT)
 Prior to box-opening, the collaboration decided to present TBA,
 which had somewhat better sensitivity. BDT analysis was used
 as a confirmation of the TBA.



$E_\nu^{QE} < 475 \text{ MeV}$ an excess of
 ν_e candidate events exists
 $128.8 \pm 20.4 \pm 38.3 (3.0\sigma)$

This excess does not fit
 a conventional 2ν oscillation
 hypothesis.

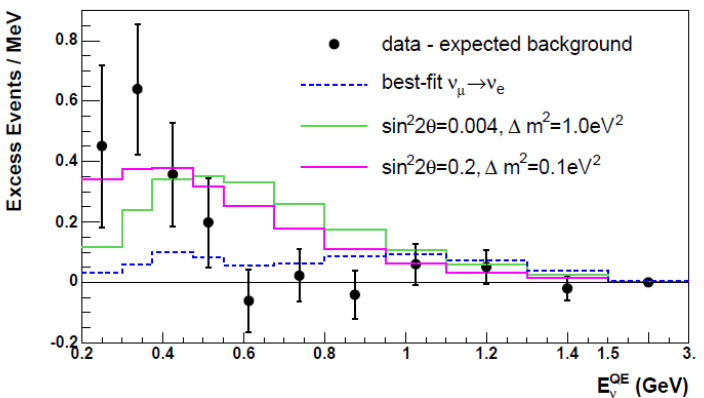
For $E_\nu^{QE} = 475 < E_\nu^{QE} < 3000 \text{ MeV}$

There is a background subtracted
 excess of ν_e candidate events of : $22 \pm 19 \pm 36$

The oscillation fit in the χ^2 probability is 93 %
 for the null hypothesis.

Compatibility with LSND is $\sim 5\%$.

The χ^2 probability is 99% for the
 best fit : $(\sin^2 2\theta = 10^{-3}, \Delta m^2 = 4eV^2)$



The excess over predicted background for
 $E_\nu^{QE} < 475 \text{ MeV}$ cannot be explained as an oscillation
 signal. It's origin is not understood,

The future:

Short baseline experiment concentrate, to some extent on searching for signs of non-interacting, or sterile neutrinos.

Many models have been proposed that profess the possible existence of this exotic form of matter.

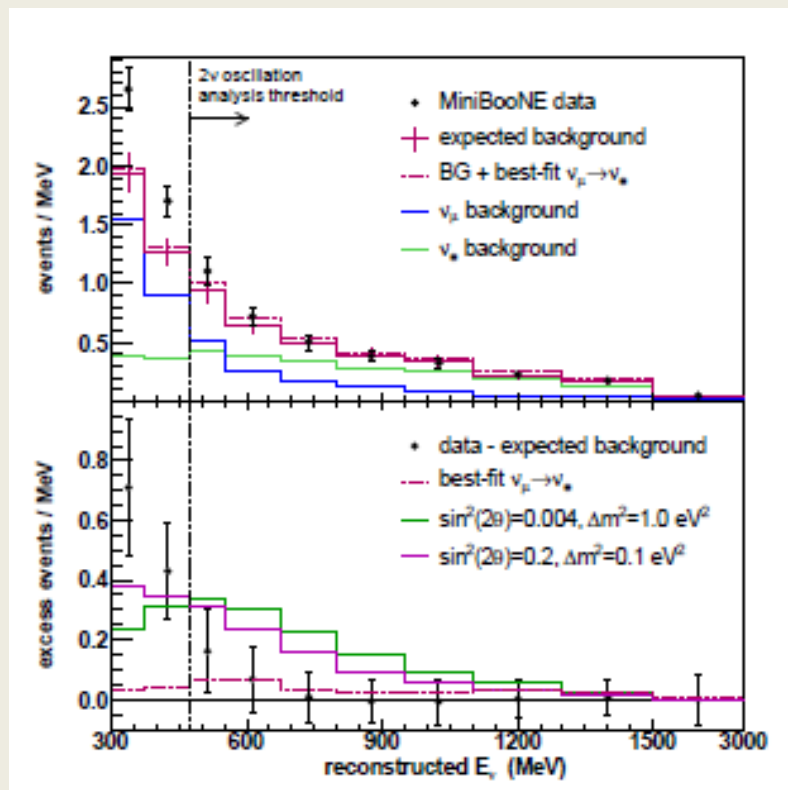
For example, the possible existence of a V+A world concurrent with ours, but not interacting because of the inverse chirality*.

More sensitive experiments, that extend current measurements to smaller values of $\sin^2(2\theta)$, may be the only method by which we can probe this otherwise invisible world.

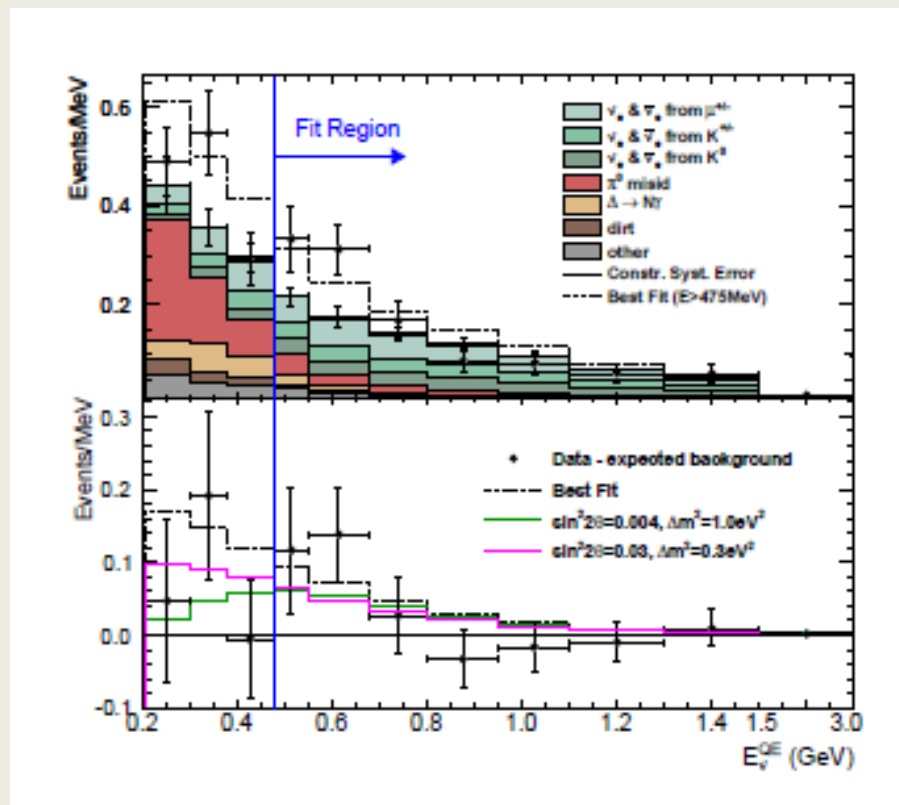
* See for example, *Introduction to Sterile Neutrinos*, Raymond R. Volkas – hep-ph/0111326 – 26 Nov 2001

Backup slides

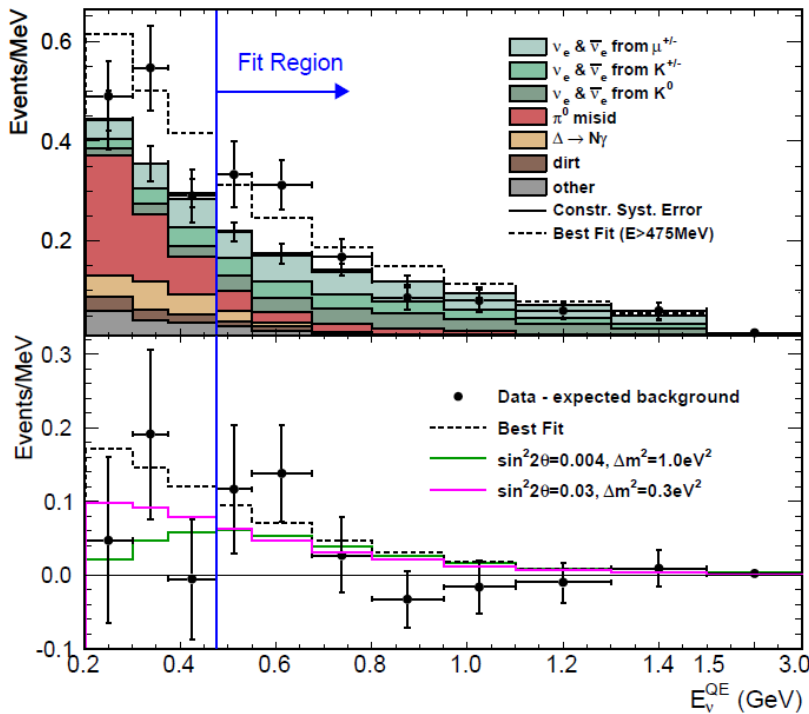
ν appearance



$\bar{\nu}$ appearance



The analysis was performed with the same tools as the TBA analysis, and the addition of a minimum likelihood fitting process. The Boosted Decision Tree (BDT) analysis is still being pursued for the anti-neutrino data.



5.33×10^{20} POT

24,771 CCQE events

22% ν

78% $\bar{\nu}$

12 events from low energy ν excess were not included in these figures

For $E_{\nu}^{\text{QE}} < 475$ MeV there is an excess of events : 18.5 ± 14.3 .

Fit Region :

An excess of events is observed : 20.9 ± 14.0 .

The oscillation fit in the $475 < E_{\nu}^{\text{QE}} < 1250$ MeV energy range yields a χ^2 probability of 8.7% for the best fit. $(\sin^2 2\theta, \Delta m^2) = (0.96, 0.64 \text{ eV}^2)$

The probability of the ratio of the likelihood of the background only fit to the likelihood of the best oscillation fit is 0.6%

Event rate was 1.9σ higher in the last 2.27×10^{20} POT than in the 1st 3.39×10^{20} .

More from MiniBooNE not covered in this talk :

- $\nu/\bar{\nu}$ disappearance analysis
combined analysis with SciBooNE
- Search for Core - Collapse Supernovae
- Analysis with the NuMI off - axis beam
- NC Elastic cross - section
- ν_{μ} and $\bar{\nu}_{\mu}$ NC single π^0 production cross sections
- ν_{μ} CC π^+ /QE Cross Section Ratio
- Coherent π^0 Production
- Limit on the Muon Neutrino Magnetic Moment

Understanding the detector: cross-sections – NUANCE

Processes available in NUANCE:

#	CC / NC	Reaction
Cabibbo-allowed quasi-elastic scattering from nucleons		
1	CC	$\nu_{\mu}n \rightarrow \mu^{-}p$ ($\bar{\nu}_{\mu}p \rightarrow \mu^{+}n$)
(Quasi-)elastic scattering from nucleons		
2	NC	$\nu_{\mu}n \rightarrow \nu_{\mu}n$ ($\bar{\nu}_{\mu}n \rightarrow \bar{\nu}_{\mu}n$) $\nu_{\mu}p \rightarrow \nu_{\mu}p$ ($\bar{\nu}_{\mu}p \rightarrow \bar{\nu}_{\mu}p$)
Resonant single pion production		
3	CC	$\nu_{\mu}p \rightarrow \mu^{-}p\pi^{+}$
4	CC	$\nu_{\mu}n \rightarrow \mu^{-}p\pi^{0}$
5	CC	$\nu_{\mu}n \rightarrow \mu^{-}n\pi^{+}$
6	NC	$\nu_{\mu}p \rightarrow \nu_{\mu}p\pi^{0}$
7	NC	$\nu_{\mu}p \rightarrow \nu_{\mu}n\pi^{+}$
8	NC	$\nu_{\mu}n \rightarrow \nu_{\mu}n\pi^{0}$
9	NC	$\nu_{\mu}n \rightarrow \nu_{\mu}p\pi^{-}$
10-16		Corresponding $\bar{\nu}_{\mu}$ processes
Multi-pion resonant processes		
17	CC	$\nu_{\mu}p \rightarrow \mu^{-}\Delta^{+}\pi^{+}$
18	CC	$\nu_{\mu}p \rightarrow \mu^{-}\Delta^{++}\pi^{0}$
19	CC	$\nu_{\mu}n \rightarrow \mu^{-}\Delta^{+}\pi^{0}$
20	CC	$\nu_{\mu}n \rightarrow \mu^{-}\Delta^{0}\pi^{+}$
21	CC	$\nu_{\mu}n \rightarrow \mu^{-}\Delta^{++}\pi^{-}$
22	NC	$\nu_{\mu}p \rightarrow \nu_{\mu}\Delta^{+}\pi^{0}$
23	NC	$\nu_{\mu}p \rightarrow \nu_{\mu}\Delta^{0}\pi^{+}$
24	NC	$\nu_{\mu}p \rightarrow \nu_{\mu}\Delta^{++}\pi^{-}$

#	CC / NC	Reaction
25	NC	$\nu_{\mu}n \rightarrow \nu_{\mu}\Delta^{+}\pi^{-}$
26	NC	$\nu_{\mu}n \rightarrow \nu_{\mu}\Delta^{0}\pi^{0}$
27	NC	$\nu_{\mu}n \rightarrow \nu_{\mu}\Delta^{-}\pi^{+}$
28-38		Corresponding $\bar{\nu}_{\mu}$ processes
39	CC	$\nu_{\mu}p \rightarrow \mu^{-}p\rho^{+}(770)$
40	CC	$\nu_{\mu}n \rightarrow \mu^{-}p\rho^{0}(770)$
41	CC	$\nu_{\mu}n \rightarrow \mu^{-}n\rho^{+}(770)$
42	NC	$\nu_{\mu}p \rightarrow \nu_{\mu}p\rho^{0}(770)$
43	NC	$\nu_{\mu}p \rightarrow \nu_{\mu}n\rho^{+}(770)$
44	NC	$\nu_{\mu}n \rightarrow \nu_{\mu}n\rho^{0}(770)$
45	NC	$\nu_{\mu}n \rightarrow \nu_{\mu}p\rho^{-}(770)$
46-52		Corresponding $\bar{\nu}_{\mu}$ processes
53	CC	$\nu_{\mu}p \rightarrow \mu^{-}\Sigma^{+}K^{+}$
54	CC	$\nu_{\mu}n \rightarrow \mu^{-}\Sigma^{0}K^{+}$
55	CC	$\nu_{\mu}n \rightarrow \mu^{-}\Sigma^{+}K^{0}$
56	NC	$\nu_{\mu}p \rightarrow \nu_{\mu}\Sigma^{0}K^{+}$
57	NC	$\nu_{\mu}p \rightarrow \nu_{\mu}\Sigma^{+}K^{0}$
58	NC	$\nu_{\mu}n \rightarrow \nu_{\mu}\Sigma^{0}K^{0}$
59	NC	$\nu_{\mu}n \rightarrow \nu_{\mu}\Sigma^{-}K^{+}$
60-66		Corresponding $\bar{\nu}_{\mu}$ processes
67	CC	$\nu_{\mu}n \rightarrow \mu^{-}p\eta$
68	NC	$\nu_{\mu}p \rightarrow \nu_{\mu}p\eta$
69	NC	$\nu_{\mu}n \rightarrow \nu_{\mu}n\eta$
70-72		Corresponding $\bar{\nu}_{\mu}$ processes
73	CC	$\nu_{\mu}n \rightarrow \mu^{-}K^{+}A$
74	NC	$\nu_{\mu}p \rightarrow \nu_{\mu}K^{+}A$
75	NC	$\nu_{\mu}n \rightarrow \nu_{\mu}K^{0}A$

Particle lifetimes & ν producing decay modes with their branching ratios

Particle	Lifetime (ns)	Decay mode	Branching ratio (%)
π^{+}	26.03	$\mu^{+} + \nu_{\mu}$	99.9877
		$e^{+} + \nu_e$	0.0123
K^{+}	12.385	$\mu^{+} + \nu_{\mu}$	63.44
		$\pi^{0} + e^{+} + \nu_e$	4.98
		$\pi^{0} + \mu^{+} + \nu_{\mu}$	3.32
K_L^0	51.6	$\pi^{-} + e^{+} + \nu_e$	20.333
		$\pi^{+} + e^{-} + \bar{\nu}_e$	20.197
		$\pi^{-} + \mu^{+} + \nu_{\mu}$	13.551
		$\pi^{+} + \mu^{-} + \bar{\nu}_{\mu}$	13.469
μ^{+}	2197.03	$e^{+} + \nu_e + \bar{\nu}_{\mu}$	100.0

A little review:

$$\begin{pmatrix} \nu_e \\ \nu_\mu \\ \nu_\tau \end{pmatrix} = \begin{pmatrix} c_{12}c_{13} & s_{12}c_{13} & s_{13}e^{-i\delta} \\ -s_{12}c_{23} - c_{12}s_{23}s_{13} & c_{12}c_{23} - s_{12}s_{23}s_{13}e^{i\delta} & s_{23}c_{13} \\ s_{12}s_{23} - c_{12}c_{23}s_{13}e^{i\delta} & -c_{12}s_{23} - s_{12}c_{23}s_{13}e^{i\delta} & c_{23}c_{13} \end{pmatrix} \begin{pmatrix} \nu_1 \\ \nu_2 \\ \nu_3 \end{pmatrix} \quad \begin{matrix} s_{ij} = \sin(\theta_{ij}) \\ c_{ij} = \cos(\theta_{ij}) \end{matrix}$$

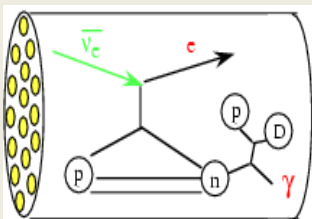
	2σ lower limit	best value	2σ upper limit	Best fit values :
$(\Delta m_{sun}^2)_{L.A.} (10^5 eV^2)$	7.14	7.67	8.19	$\sin \theta_{12} = .56$ $\cos \theta_{12} = .83$
$\Delta m_{atm}^2 (10^3 eV^2)$	2.06	2.39	2.81	$\sin \theta_{23} = .68$ $\cos \theta_{23} = .73$
$\sin^2 \theta_{12}$.263	.312	.375	$\sin \theta_{13} = .13$ $\cos \theta_{13} = .992$
$\sin^2 \theta_{23}$.331	.466	.644	
$\sin^2 \theta_{13}$	0	$\leq .0046$	(0.016 ± 0.010)	

Carl Albright, November 12, 2009

Majorana condition?

$$\nu = \nu^c$$

↯ 2-β decay



No room for additional ν

$$\Delta m_{LSND}^2 \approx 1/2 eV^2$$

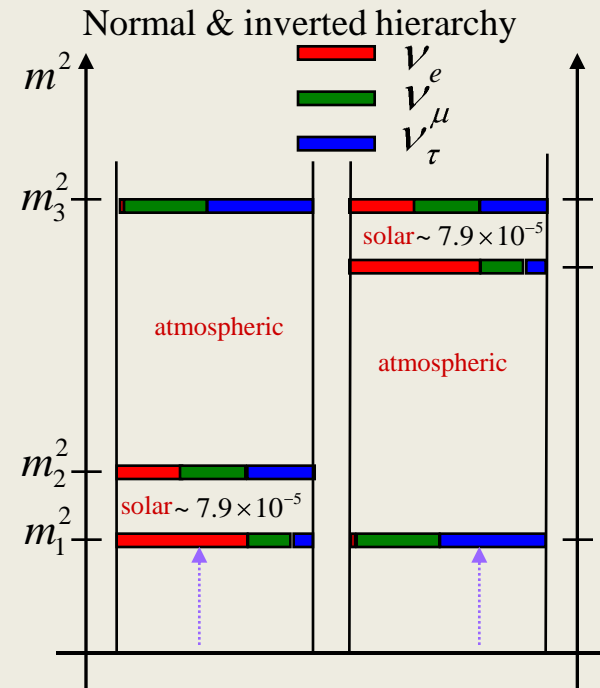
$$\Delta m_{13}^2 = \Delta m_{12}^2 + \Delta m_{23}^2$$

Plugging in the best fit values:

$$(|U_{lv}|^2) = \mu \begin{matrix} & \nu_1 & \nu_2 & \nu_3 \\ e & (.68 & .31 & .016) \\ \mu & (.23 & .31 & .46) \\ \tau & (.09 & .38 & .53) \end{matrix}$$

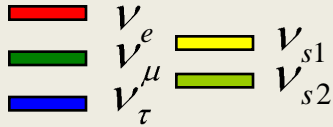
Tri-bimaximal mixing:

$$(|U_{lv}|^2) = \mu \begin{matrix} & \nu_1 & \nu_2 & \nu_3 \\ e & (.67 & .33 & 0) \\ \mu & (.17 & .33 & .5) \\ \tau & (.17 & .33 & .5) \end{matrix}$$

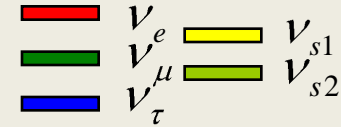
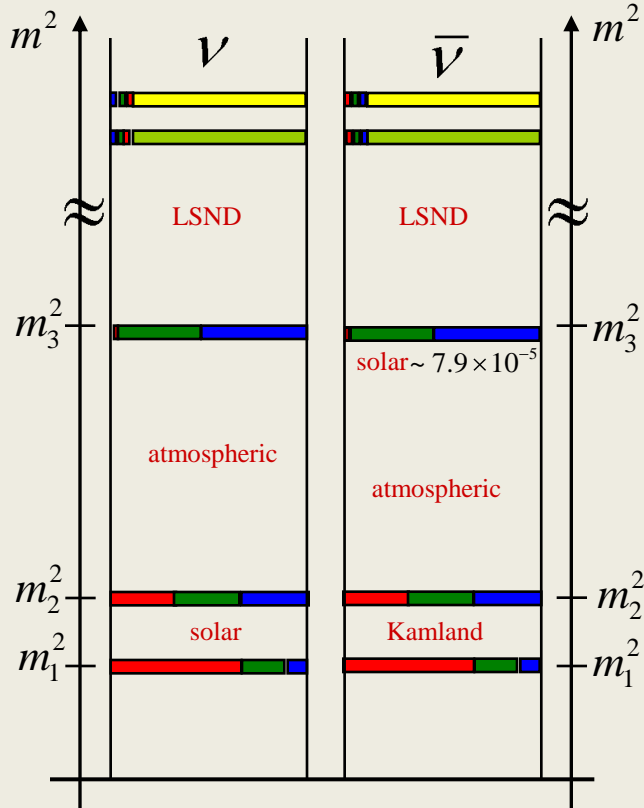


Sterile neutrinos

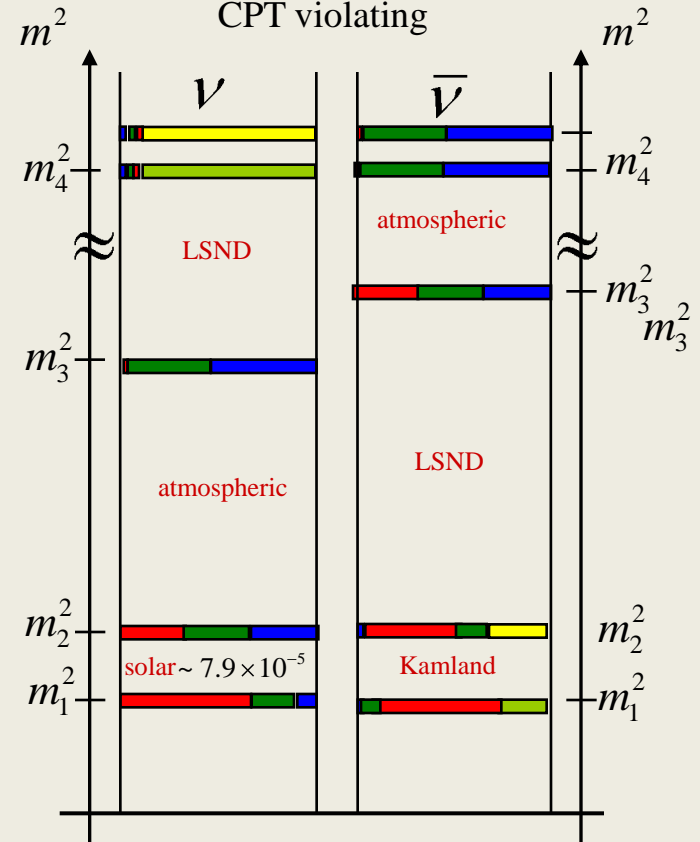
- (3+1) schemes cannot accommodate existing measurements.
- (3+2) schemes are still viable.
- CPT non-conservation can apply to any (3+N) scheme.



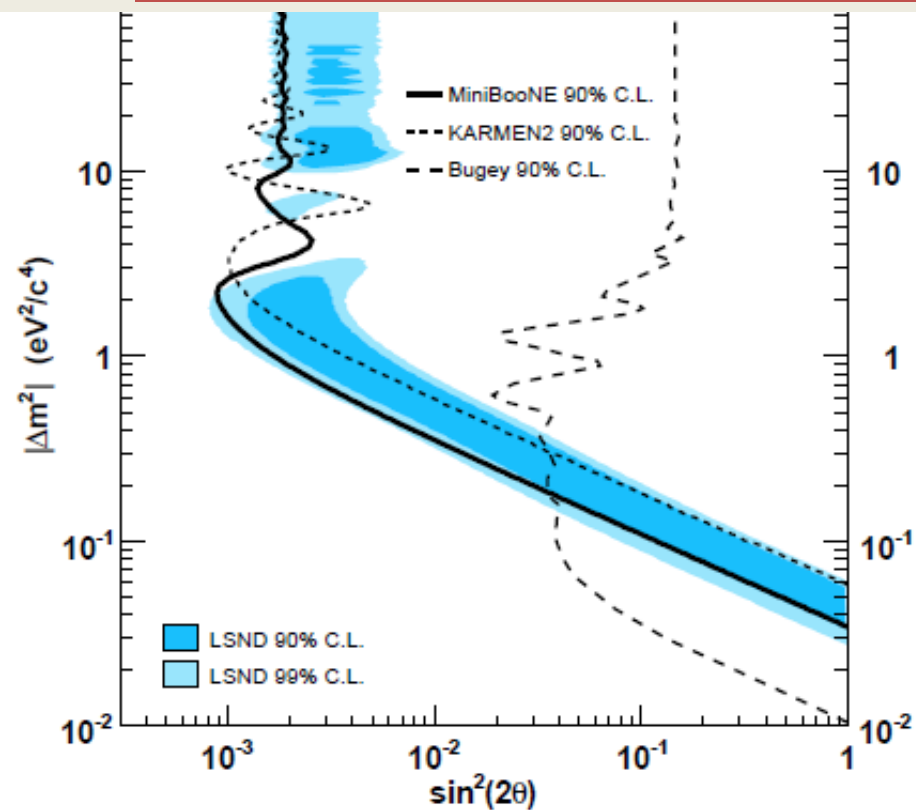
CPT conserving



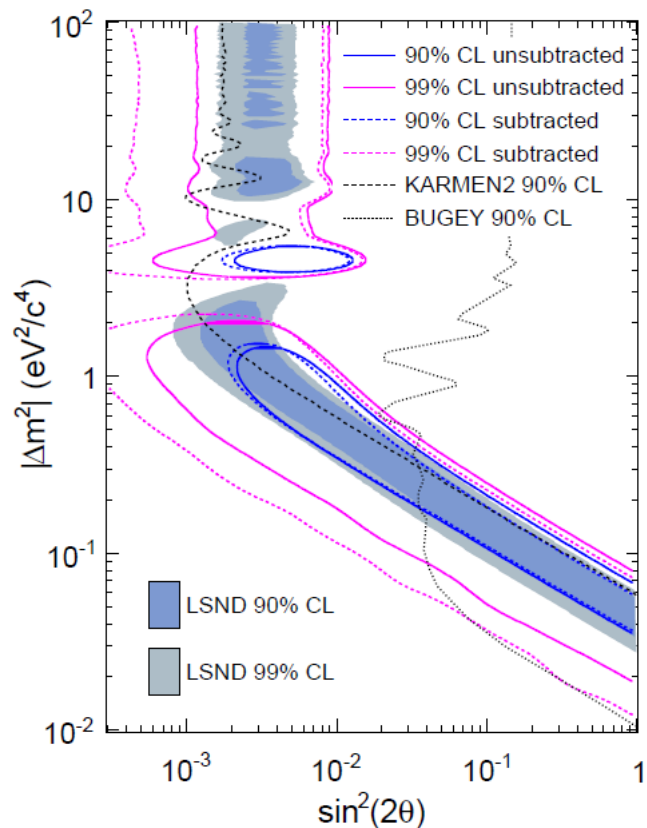
CPT violating



$\nu / \bar{\nu}$ appearance

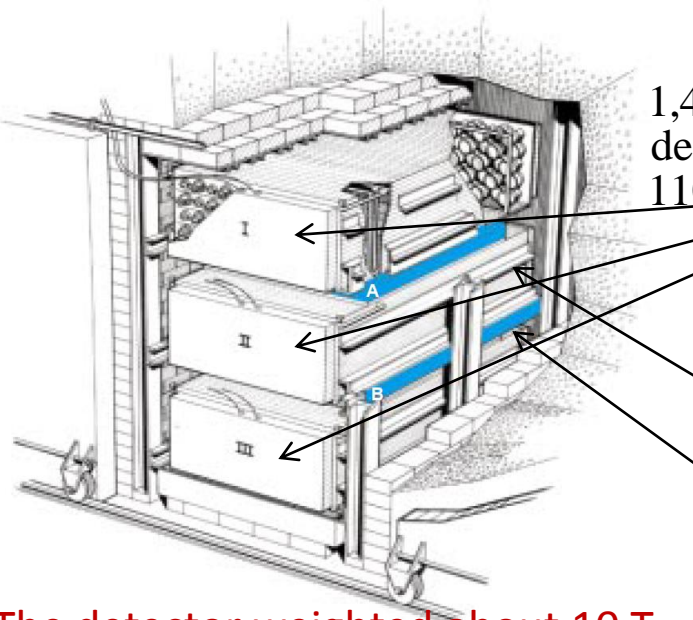


MiniBooNE 90% CL limit (dark solid curve) compared to KARMEN and Bugey experiments.



MiniBooNE 90% and 99% CL allowed regions compared to KARMEN and Bugey experiments.

Savannah River Neutrino Detector, circa 1955

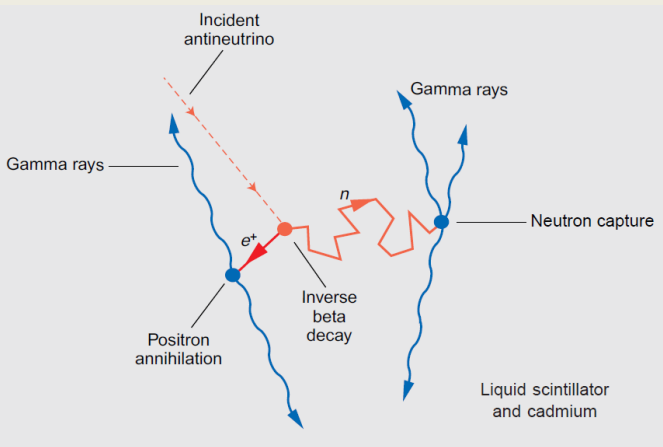


1,400 liter scintillator detectors, viewed by 110 PMTs.

200 liter water targets, doped with $CdCl_2$

β decay in reactor creates an intense beam of $\bar{\nu}_e$.
 In detector:
 $\bar{\nu}_e + p \rightarrow e^+ + n$
 $n + p \rightarrow d + \gamma(2.2MeV)$
 Dalitz pair: $e^+ + e^- \rightarrow \gamma + \gamma$:
 EM shower: $\gamma(2.2MeV)$
 The excited $CdCl_2$ nucleus has a lifetime $\sim 3 \mu s$.

The detector weighted about 10 T.

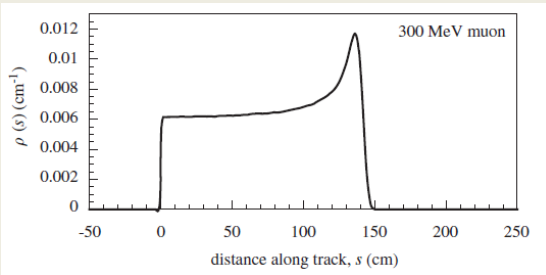


attributes :
 $S/N \sim 4/1$
 $\langle E \rangle = 3 \text{ MeV}$
 $\text{flux} = 10^3 \bar{\nu}_e / \text{cm}^2 \text{ s}$
 $\sigma = 6 \times 10^{-44} \text{ cm}^2$
 inverse β decay prior to discovery of V - A.

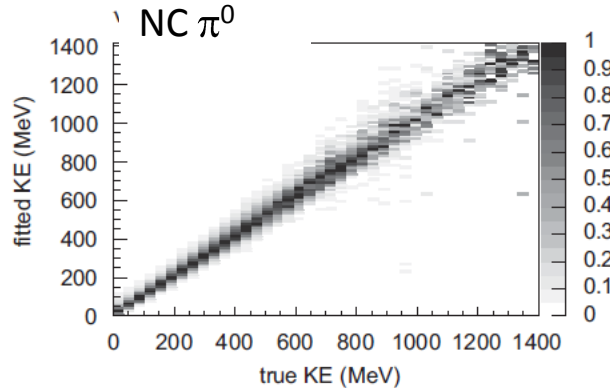
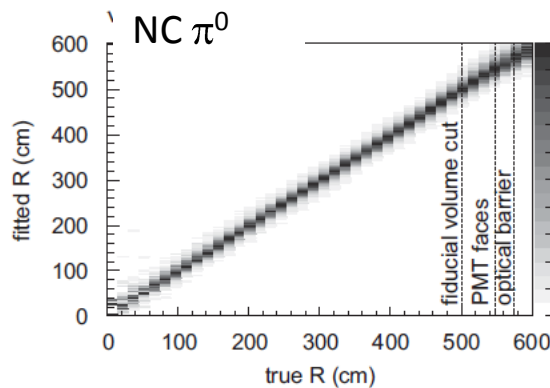
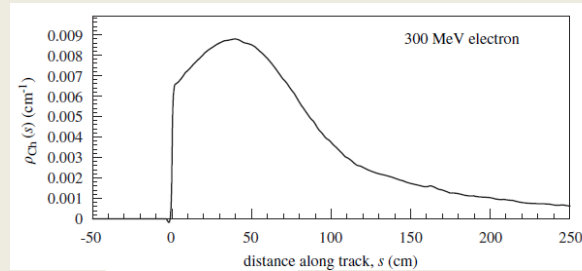
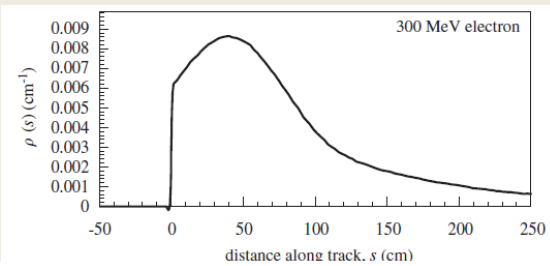
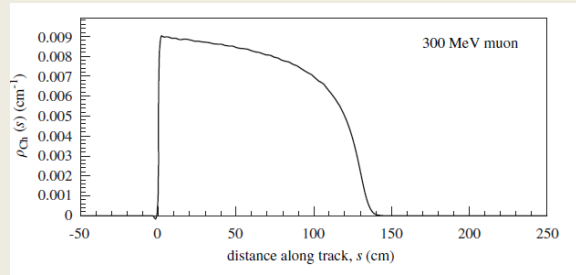
This technique is still used in reactor experiments, the observation of two distinct signatures separated in time by a known amount.

MiniBooNE Sources of systematic uncertainties: charge likelihood

Scintillation Emission Profiles generated in simulation.

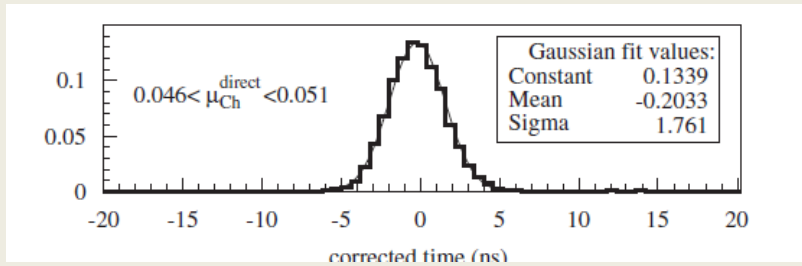


Cherenkov Emission Profiles generated in simulation.

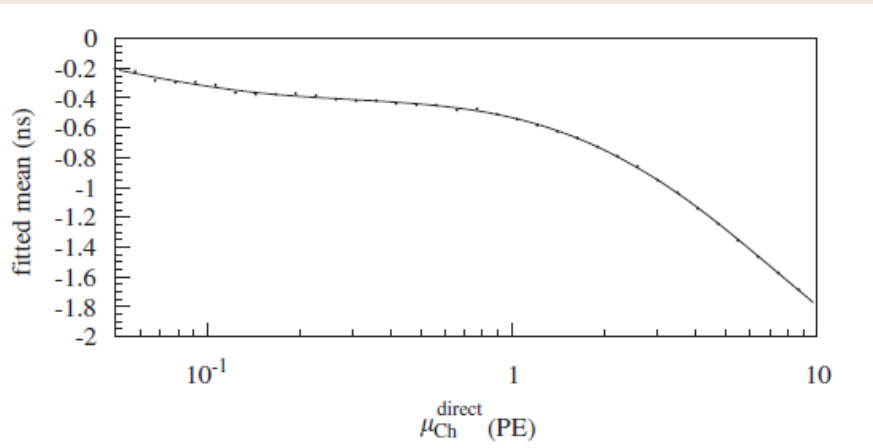


To these we must add the effects of indirect light from scattering, fluorescence, etc.

MiniBooNE event reconstruction – time likelihood:



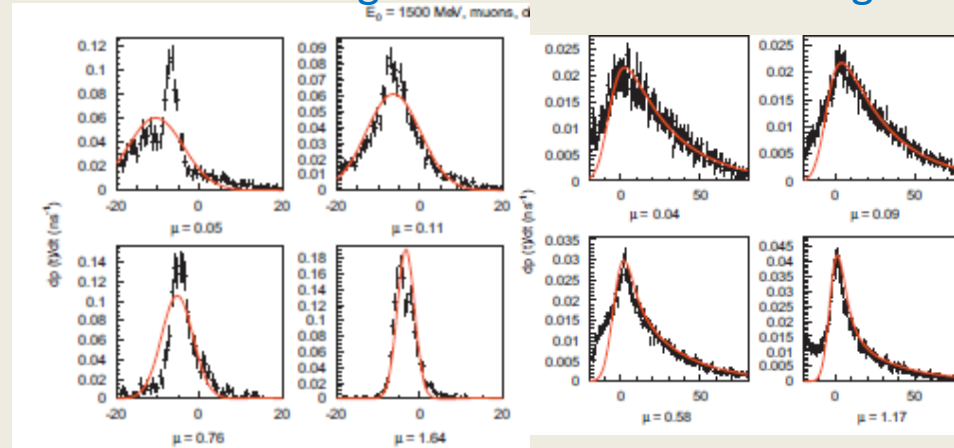
Distribution of corrected time for direct light, can be fit with Gaussian mean and width.



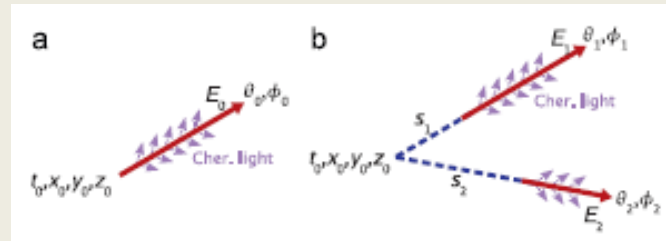
For 300 MeV muons, the mean and width parameters from fits like those above vs. direct Cherenkov predicted charge.

Using the known optical photon and Particle optical properties of the detector, one determines for a given particle type (e/μ) and a set of track parameters, the average number of pe's that a particular PMT should observe. This quantity is referred to as the predicted charge.

$E_0 = 1500$ MeV Cherenkov light Scintillation light



Parameterized t^c likelihood distributions as a function of predicted charge.



Internal fit parameters for (a) a single track and (b) two photon tracks. Each photon track contains a conversion distance parameter s .

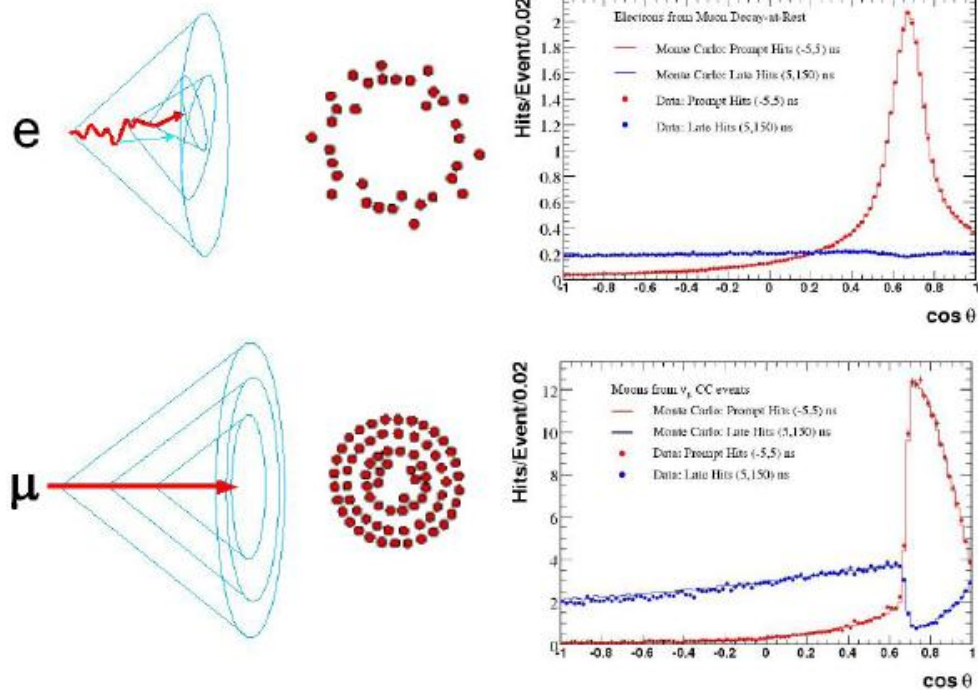


Figure 6.6: Cherenkov light patterns of electrons and muons in the MiniBooNE detector. The right plots show the angular distribution of PMT hits with respect to the electron or muon direction. Red points (data) and histograms (MC) are the prompt Cherenkov light. Blue points (data) and histograms (MC) are the contribution from more delayed scintillation light.

were detected in the MiniBooNE oil [89] and their individual time constants represent 4 more parameters of the optical model. Their scintillation, fluorescence and UV fluorescence⁵ photon yields are 12 more. However, data rich in scintillation light (NC elastic scattering events) used to calibrate the model prefer the use of a single fluorophore with a time constant $\tau = 34$ ns. The other three are used to assess systematic errors. The number of scintillation photons produced per unit deposited energy is simulated according to

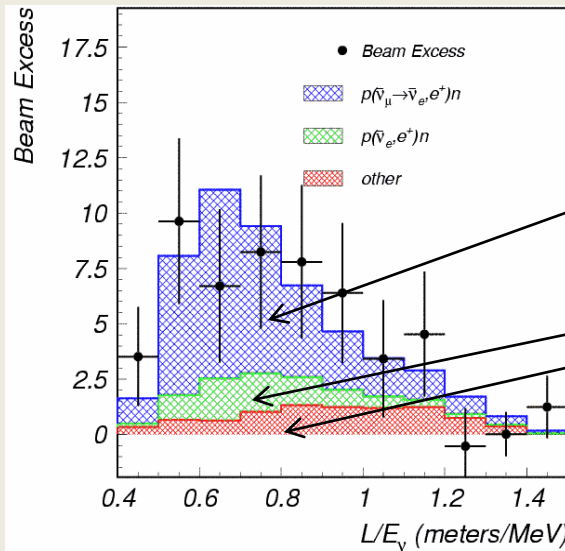
$$\frac{dN_{\text{Sci}}}{dE} = \frac{31.64 \text{ MeV}^{-1}}{1 + B_1 \left(\frac{1}{\rho_{\text{oil}}} \frac{dE}{dx} \right) + B_2 \left(\frac{1}{\rho_{\text{oil}}} \frac{dE}{dx} \right)^2} \quad (7.15)$$

with $B_1 = 0.014 \text{ g}/(\text{MeV} \cdot \text{cm}^2)$ and $B_2 = 0.0 \text{ g}^2/(\text{MeV}^2 \cdot \text{cm}^4)$. B_2 is included only for the purposes of assessing systematic errors. This is known as Birks' Law and constitutes 2 of the 35 parameters of the detector optical model.

Liquid Scintillator Neutrino Detector

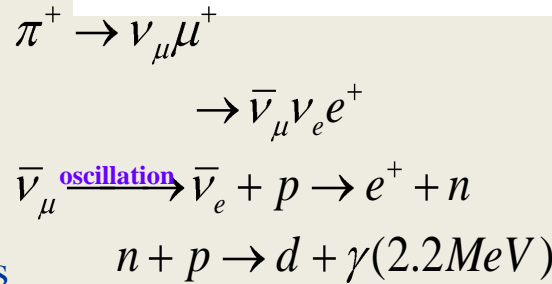
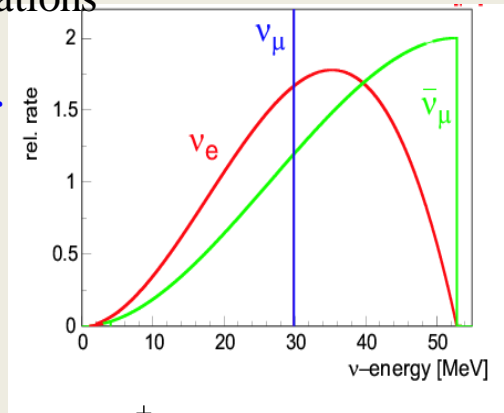
LSND observed an excess of $\bar{\nu}_e$ events = $87.9 \pm 22.4 \pm 6.0$ (3.8σ)
 which might be interpreted as $\bar{\nu}_\mu \rightarrow \bar{\nu}_e$ oscillations

attributes :
 S/N ~ 4/1
 $\langle E \rangle = \leq 50 \text{ MeV}$
 $\sigma \cong 10^{-42} \text{ cm}^2$
 inverse β decay



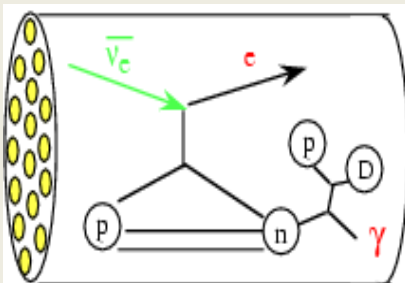
Expectation for oscillations
 $(\Delta m^2 = 0.24 \text{ eV}^2)$

Beam-related backgrounds



The absolute mass scale, determined from combined WMAP, SDSS, and Lyman alpha data places an upper limit on the sum of the ν masses.
 $\sum_i m_i \leq 0.17 - 1.2 \text{ eV}^2$.

- Similar in technique to reactor experiments
- A source of stopping μ 's
- Energy spectrum of all decay products well known
- 2.2 MeV γ from neutron capture rejects ν_e



800 MeV energy 1-mA intensity
 167 T mineral oil
 14 lbs of scintillating material
 1220 PMTs
 accidental γ are backgrounds.

Similar experiments that fail to observe the LSND result:
 BNL E776(counter)
 Karmen(ISIS)
 Bugey(reactor)

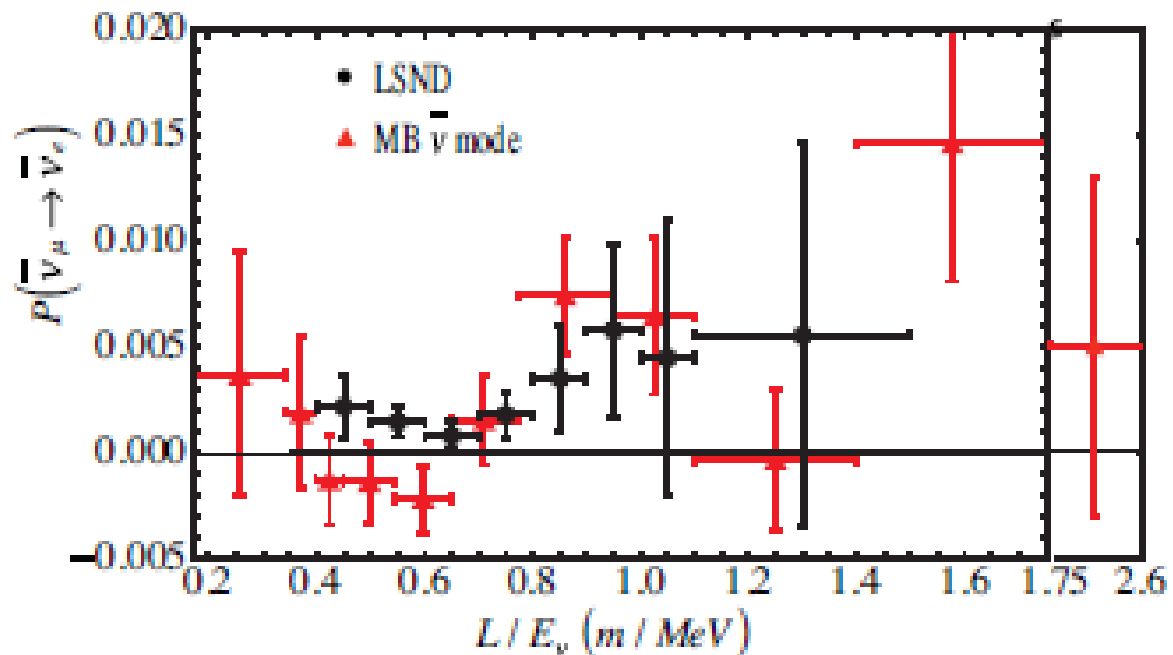


FIG. 5: The oscillation probability as a function of L/E_ν^{QE} for $\bar{\nu}_\mu \rightarrow \bar{\nu}_e$ candidate events from MiniBooNE and LSND. The data points include both statistical and systematic errors.

This is basically a talk about sterile neutrinos:

Let's look first at the See-Saw mechanism

The smallness of the neutrino mass may be the result of mixing between Dirac and Majorana mass terms in the Electroweak Lagrangian. If we assume no Majorana neutrinos, the Lagrangian takes the form:

$$\mathcal{L} = i\bar{\nu}\gamma_\mu\partial_\mu\nu - m\bar{\nu}\nu, \text{ where}$$

$$\nu = \nu_L + \nu_R \quad \bar{\nu} = \bar{\nu}_L + \bar{\nu}_R$$

$$\mathcal{L}^D = -m_D\bar{\nu}\nu = -m_D(\bar{\nu}_R\nu_L + \bar{\nu}_L\nu_R) ; \bar{\nu}_L\nu_L = 0 ; \bar{\nu}_R\nu_R = 0$$

The Majorana condition states that the neutrino is the same particle as its anti - neutrino

$$\nu_R = \nu_L^c = C\bar{\nu}_L^T ; \nu_L = \nu_R^c = C\gamma^{0T}\bar{\nu}_R^T, \text{ where C is the charge conjugation operator.}$$

That is, Majorana particles are the same as the corresponding antiparticles.

This introduces new mass terms into the EW Lagrangian :

$$\mathcal{L}_L^M = -\frac{1}{2}m_R(\bar{\nu}_L^c\nu_L + \bar{\nu}_L\nu_L^c) ; \nu_R = \nu_L^c$$

$$\mathcal{L}_R^M = -\frac{1}{2}m_R(\bar{\nu}_R^c\nu_R + \bar{\nu}_R\nu_R^c) ; \nu_L = \nu_R^c$$

When we combine the Dirac and Majorana terms, we get a sum of four terms :

$$\mathcal{L}^{D+M} = \mathcal{L}^D + \mathcal{L}_L^M + \mathcal{L}_R^M =$$

$$-\frac{1}{2}m_D(\bar{\nu}_R\nu_L + \bar{\nu}_L\nu_R) - \frac{1}{2}m_D(\bar{\nu}_R\nu_L + \bar{\nu}_L\nu_R) - \frac{1}{2}m_R(\bar{\nu}_R^c\nu_R + \bar{\nu}_R\nu_R^c) - \frac{1}{2}m_R(\bar{\nu}_L^c\nu_L + \bar{\nu}_L\nu_L^c) = -\frac{1}{2}\begin{pmatrix} \bar{\nu}_L^c & \bar{\nu}_R^c \end{pmatrix} \bar{N}_R \begin{pmatrix} m_L & m_D \\ m_D & m_R \end{pmatrix} \begin{pmatrix} N_L \\ N_R^c \end{pmatrix}$$

When we diagonalize the mass matrix we get a see-saw configuration:

$$\tan 2\theta = \frac{2m_D}{m_R - m_L} ; m_1 \approx m_R ; m_2 \approx \left(\frac{m_D^2}{m_R} \right) ; \text{ where we assumed } m_L = 0.$$

Cube depth (cm)	X (cm)	Y (cm)	Z (cm)	$\langle T_\mu \rangle$ (MeV)
31.3	-60.8	540.7	15.1	95.0 ± 4.0
60.3	15.6	511.7	-57.6	155.0 ± 5.0
100.5	57.9	471.5	-13.5	229.0 ± 7.0
200.8	-18.6	371.2	59.2	407.0 ± 9.0
298.1	40.8	273.9	44.5	584.0 ± 9.0
401.9	40.8	170.1	44.5	771.0 ± 9.0

Table 4.4: Positions of cosmic muon calibration cubes. $\langle T_\mu \rangle$ is the average kinetic energy of muons stopped in the cube.

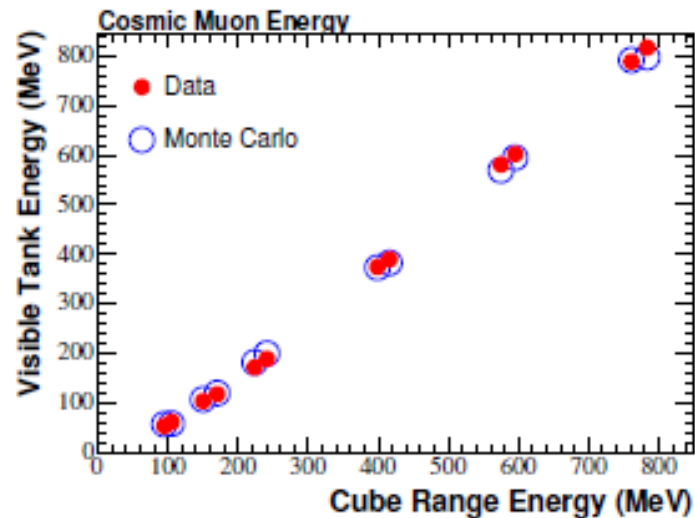


Figure 4.12: Muon energy calibration from the cosmic muon calibration system. The visible energy is from the *StancuFitter* electron hypothesis, since there was no muon hypothesis fitter at the time of the calibration measurement.

Example: Sterile neutrinos can enter SUSY models through the See-Saw mechanism

Takahashi and Tanimototo [arXiv:07040186]

The authors developed a model using the mass varying neutrinos of Fardon, Nelson & Weiner, JCAP, **0410**, 005 (2004), in which the left handed Majorana is also massive, and a sterile neutrino plays a part. The authors assume a chiral super-field, A, in dark matter. The superfield A couples to both the left-handed lepton doublet super-field L, and the right-handed neutrino super-field R. The authors introduce a scalar potential of the form:

$$V(\phi) = \frac{\lambda^2}{4} |\phi|^4 + M_A^2 |\phi|^2 + m_D^2 |\phi|^2, \text{ leads to a Lagrangian :}$$

$$\mathcal{L} = n\lambda\phi_a n + nM_A n + \bar{\nu}_L m_D n + \bar{\nu}_L M_D \nu_R + \bar{\nu}_R M_R \nu_R + h.c.$$

The mass matrix becomes :

$$\mathcal{M} \cong \begin{pmatrix} -\frac{M_D^2}{M_R} & m_D \\ m_D & M_A + \lambda\langle\phi\rangle \end{pmatrix}, \text{ in the basis } (\nu_L n), \text{ and yields mass eigenvalues of the form :}$$

$$m_{\nu_L} = \frac{-\frac{M_D^2}{M_R} + M_A + \lambda\langle\phi\rangle}{2} + \frac{\sqrt{\left[\frac{M_D^2}{M_R} + (M_A + \lambda\langle\phi\rangle)\right]^2 + 4m_D^2}}{2}$$

$$m_n = \frac{-\frac{M_D^2}{M_R} + M_A + \lambda\langle\phi\rangle}{2} - \frac{\sqrt{\left[\frac{M_D^2}{M_R} + (M_A + \lambda\langle\phi\rangle)\right]^2 + 4m_D^2}}{2}$$

λ is a coupling constant

M_A , M_D , M_R , and m_D are mass parameters

The scalar and spinor component of A are ϕ and n.

The scalar component ϕ corresponds to the acceleron causing the present cosmic acceleration.

The spinor component n is a sterile neutrino.

Understanding the detector: Sanford-Wang formula

$$\frac{d^2\sigma}{dpd\Omega}(p, \theta) = c_1 p^{c_2} \left(1 - \frac{p}{p_B - c_9} \right) \exp \left(c_3 \frac{p^{c_4}}{p_B^{c_8}} - c_6 \theta (p - c_7 p_B \cos^{c_8} \theta) \right),$$

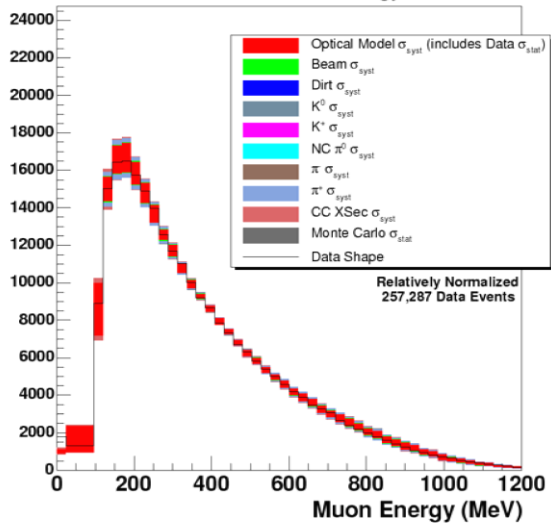
where $\frac{d^2\sigma}{dpd\Omega}$ is the double differential cross section,

p is the total momentum of the muon,

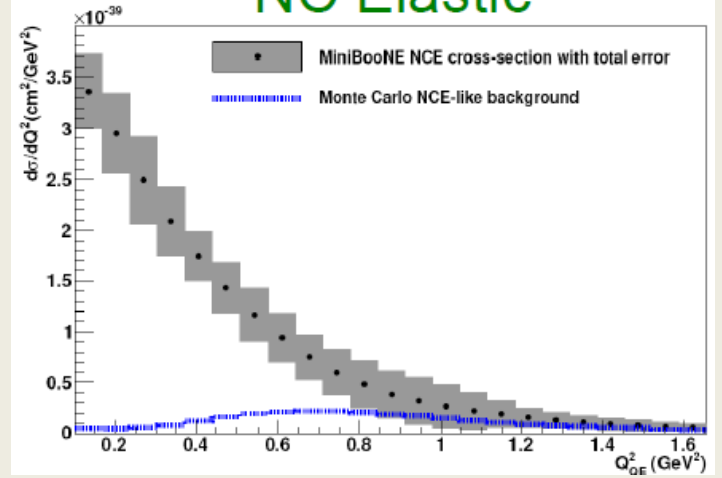
p_B is the momentum of the incident proton, and

$c_{1,\dots,9}$ are parameters determined by the fit to production data.

Reconstructed Muon Energy

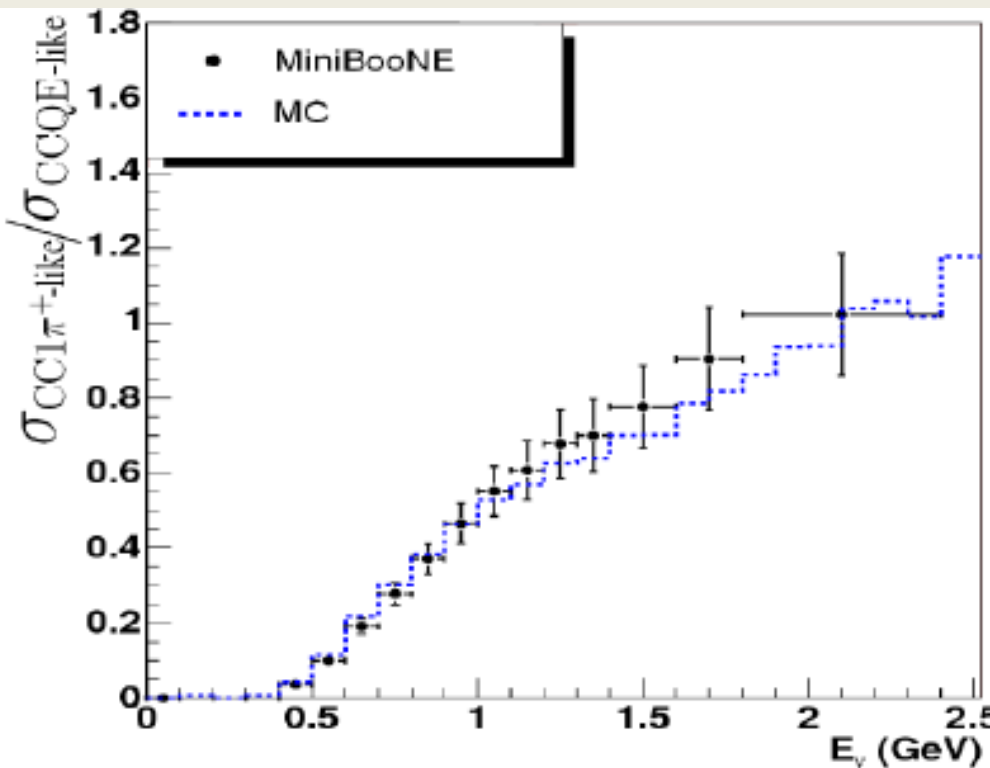


NC Elastic



Results: cross sections:

CC π^+ / CCQE ratio



Observed CC1 π^+ - like/CCQE - like cross - section ratio on CH_2 , including both statistical and systematic uncertainties, compared with simulation. The data have not been corrected for hadronic - reinteraction.

CC π^0 / CCQE ratio

